AD-A180 354 FATIGUE CRACK-GROWTH RESISTANCE OF ALUMINUM ALLOYS 1/1
UNDER SPECTRUM LOADING (U) NORTHROP CORP HAWTHORNE CA
AIRCRAFT GROUP G V SCARICH ET AL DEC 85
UNCLASSIFIED NOR-85-141-VOL-1 N00014-82-C-0425 F/G 11/6 1 NL

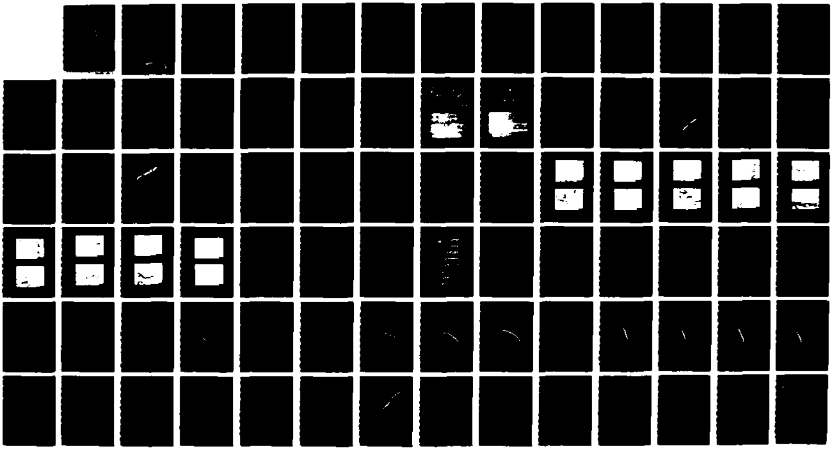

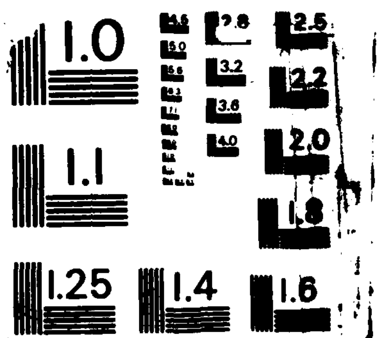

MICROCOPY RESOLUTION TEST CHART

NATIONAL BUREAU OF STANDARDS-1963-A

DTIC FILE COPY

AD-A180 354

FATIGUE CRACK-GROWTH RESISTANCE OF ALUMINUM ALLOYS UNDER SPECTRUM LOADING
Volume I — Commercial 2XXX and 7XXX Alloys

G. V. SCARICH
P. E. BRETZ

DECEMBER 1985
NOR 85-141

TECHNICAL REPORT
FINAL REPORT FOR PERIOD 30 SEPTEMBER 1982 THROUGH 31 MARCH 1985
CONTRACT NO. N00019-82-C-0425

DEPARTMENT OF THE NAVY
NAVAL AIR SYSTEMS COMMAND
WASHINGTON, D.C. 20361

NORTHROP
Aircraft Division
Aircraft Group
Northrop Corporation
One Northrop Avenue
Hawthorne, California 90250

87-5-11-023

6a. NAME OF PERFORMING ORGANIZATION Northrop Corporation Aircraft Division	6b. OFFICE SYMBOL (If applicable)	7a. NAME OF MONITORING ORGANIZATION Naval Air Systems Command
6c. ADDRESS (City, State and ZIP Code) One Northrop Avenue Hawthorne, California 90250		7b. ADDRESS (City, State and ZIP Code) Department of the Navy Washington, DC 20301
8a. NAME OF FUNDING/SPONSORING ORGANIZATION Naval Air Systems Command	8b. OFFICE SYMBOL (If applicable)	9. PROCUREMENT INSTRUMENT IDENTIFICATION NUMBER N00019-82-C-0425
8c. ADDRESS (City, State and ZIP Code) Department of the Navy Washington, D.C. 20361		10. SOURCE OF FUNDING NOS. PROGRAM ELEMENT NO. | PROJECT NO. | TASK NO. | WORK UNIT NO.
11. TITLE (Include Security Classification) See Cover		
12. PERSONAL AUTHOR(S) G.V. Scarich (Northrop) P.E. Bretz (Alcoa)		
13a. TYPE OF REPORT Technical Report	13b. TIME COVERED FROM 30 Sept 82 TO 31 Mar 85	14. DATE OF REPORT (Yr., Mo., Day) December 1985 — 15. PAGE COUNT 77
16. SUPPLEMENTARY NOTATION Volume II of this report, "Aluminum Lithium Alloys" contains the results of the balance of the effort of this contract.		

17. COSATI CODES			18. SUBJECT TERMS (Continue on reverse if necessary and identify by block number)			
FIELD	GROUP	SUB. GR.	2020	7075	Aluminum Alloys	Microstructure
			2024	7475	Fatigue	Fracture Toughness
			2124	7050	Spectrum Loading	Constant-Amplitude Loading
			2324	7150	Retardation	Variable-Amplitude Loading

19. ABSTRACT (Continue on reverse if necessary and identify by block number)

The purpose of this program is to obtain metallurgical guidelines and test methodologies for selection and development of spectrum fatigue-resistant, high-strength aluminum alloys for application to aircraft structures. This volume (I) of this report describes the results of baseline characterizations of two high-strength aluminum alloys, and compares these results to those obtained in the two previous phases of the program.

Twelve commercial 2XXX and 7XXX aluminum alloys were chosen and characterized for chemical composition, microstructure, tensile properties, and fracture toughness. Fatigue crack propagation (FCP) tests were conducted on specimens of each alloy for both constant-amplitude loading (including the near-threshold region) and two F-18 load spectrums. One of the spectrums was dominated by tension loads and the other contained tension and compression loads of nearly equal magnitude. The spectrum FCP testing was performed at the maximum peak stress of 145 MPa (21 ksi) with limited testing at 103 and 169 MPa (15 and 24.5 ksi) to obtain additional data at the low and high end of the crack-growth range. Pertinent fracture surface features were documented on the spectrum fatigue specimens.

20. DISTRIBUTION/AVAILABILITY OF ABSTRACT UNCLASSIFIED/UNLIMITED ☒ SAME AS RPT. ☐ DTIC USERS ☐	21. ABSTRACT SECURITY CLASSIFICATION UNCLASSIFIED	
22a. NAME OF RESPONSIBLE INDIVIDUAL W. L. Koegel	22b. TELEPHONE NUMBER (Include Area Code) (212) 692-6025	22c. OFFICE SYMBOL NAVAIR-530486

19. Abstract (continued)

For fatigue crack-growth testing under constant amplitude loading, the significant observations were that (1) the differences in fatigue crack-growth rates were greatest in the near-threshold regime, where 2024-T351, 2124-T351, and 7475-T651 showed the highest resistance to FCP and (2) FCP resistance varied with the stress intensity factor range (ΔK). For example, in contrast to its excellent near threshold crack-growth resistance, 7475-T651 had the lowest resistance to FCP for ΔK greater than 6 MPa $\sqrt{m}$.

For spectrum testing at the maximum peak stress of 145 MPa (21 ksi):

1. The ranking of the alloys by spectrum life is the same for both spectrums, except for 2020-T651. The alloys ranked as follows with their percentage of life relative to 2124-T351, averaged for both spectrums, shown in parentheses: 2124-T351 (100%), 2024-T351 (81%), 7475-T651 (76%), 2324-T39 (72%), 2020-T651 (70%), 7475-T7351 (64%), 7050-T7451 (63%), 7150-T6E189 (55%), 7075-T7351 (53%), 2124-T851 (46%), 7075-T651 (44%), and 2024-T851 (35%).

2. For each material the tension-dominated spectrum consistently resulted in longer lives than the tension-compression spectrum.

Eight of the ten alloys were spectrum fatigue tested using two independent modifications of the baseline spectrums. One modification, the racetrack method, was used to eliminate 43 percent of the low-amplitude cycles to reduce testing time. The differences in spectrum fatigue lives between the modified and baseline spectrums were small enough so that the selection of one alloy over another would not be significantly affected.

The second modification was made to determine the importance of compressive load cycles. To accomplish this, all compression load points were eliminated from the tension-compression spectrum. There were significant increases in spectrum lives compared to the baseline spectrum, but the ranking of the eight alloys for this modified spectrum was identical to that for the baseline spectrum except for 2020-T651 which changed from fifth to second.

In general, the spectrum performance rankings could not be correlated with yield strength or constant-amplitude FCP resistance. However, spectrum performance could be correlated with fracture toughness. Specifically for the testing at 145 and 169 MPa, FCP life for both spectrums generally increased with increased fracture toughness. Also the alloys that deform by planar slip generally had longer spectrum fatigue lives than those that deformed more homogeneously. The effects of deformation mode and grain structure were evaluated by producing alloys with controlled variations in chemistry, aging, and thermomechanical processing. These results are reported in Volume II of this report entitled "Spectrum Fatigue Crack-Growth Resistance of Aluminum Alloys Under Spectrum Loading-Aluminum Lithium Alloys."

PREFACE

This report was prepared by the Northrop Corporation, Aircraft Division, Hawthorne, California, under Naval Air Systems Command Contract N00019-82-C-0425. Ms. G. Weaver of Naval Air Systems Command (Code AIR-5304B4) was the project engineer.

Northrop Corporation, Aircraft Division, was the prime contractor, with Mr. G.V. Scarich serving as the program manager. Mr. K.M. Bresnahan was involved in the analysis of the deformation behavior, which included the correlation of fracture features with microstructure. Mr. S. Hsu was responsible for all the spectrum testing and data reduction, while Mr. P.G. Porter was responsible for spectrum selection, generation, and modification.

Aluminum Company of America, Alcoa Technical Center, was a major participant in the program. Dr. P.E. Bretz served as the Alcoa program manager and Principal Investigator. Alcoa was intimately involved in all the phases of the program and was primarily responsible for determination of baseline mechanical properties, microstructural characterization, and fracture surface/microstructure interpretation.

The contractor report number is NOR 84-141. This report covers work from 30 September 1982 through 31 March 1985, and it consists of two volumes:

Volume I – Commercial 2XXX and 7XXX Alloys

Volume II – Aluminum Lithium Alloys.

The authors also wish to acknowledge R. Schmidt formerly of NAVAIR; A.P. Divecha of NSWC; and B.J. Mays, A.H. Freedman, G.R. Chanani, S.W. Averill, J. Luck, D.R. Drott, J.P. Bouffard, and J.M. Wilson of Northrop; and J.T. Staley and R.R. Sawtell of Alcoa for their cooperation and support during the various phases of the program.

CONTENTS

ILLUSTRATIONS

ILLUSTRATIONS (Continued)

TABLES

ABBREVIATIONS AND SYMBOLS

a	Crack-length
a_i	Initial crack length
a_c	Current crack length
a_f	Final crack length
B	Specimen thickness
COD	Crack opening displacement
da/dH	Spectrum crack growth rate
da/dN	Crack growth rate (constant amplitude)
F	Failure
FCGR	Fatigue crack growth rate
FCP	Fatigue crack propagation
H	Simulated flight hours or half height of compact tension specimen
K	Stress-intensity factor
K_{eff}	Effective stress intensity
K_{hmax}	Stress-intensity factor at largest (highest) peak of spectrum
K_{hmin}	Stress-intensity factor at smallest (lowest) valley of spectrum
K_{max}	Maximum stress intensity factor
K_{Ic}	Plane strain fracture toughness
K_Q	Conditional fracture toughness; test did not meet all the ASTM E399 validity criteria
L	Longitudinal
L-T	Crack growth on plane normal to the rolling direction (L) of the plate in a direction transverse (T) to the rolling direction (per ASTM E399)
N	Number of cycles
P	Load
P_{cl}	Crack closure load
P_{hmax}	Load at largest (highest) peak of a spectrum
P_{hmin}	Load at smallest (lowest) valley in a spectrum
P_{max}	Peak load
P_{sm}	Mean spectrum load

ABBREVIATIONS AND SYMBOLS (Concluded)

R	Stress or load ratio = P_{min}/P_{max}
SEM	Scanning electron microscope/microscopy
SFCGR	Spectrum fatigue crack growth rate
TC	Tension-compression, horizontal hinge tail moment spectrum
TCR	Racetrack-modified, tension-compression spectrum
TC(R)	Average of TC and TCR spectrum lives
TCZ	Tension-compression-zero spectrum
TD	Tension-dominated, lower wing root spectrum
TDR	Racetrack-modified, tension-dominated spectrum
TD(R)	Average of TD and TDR spectrum lives
TEM	Transmission electron microscope/microscopy
T/2	Mid-thickness (center) location in a plate
T/4	Quarter-thickness location in a plate
3T/4	Three-quarter thickness location in a plate
W	Specimen width
YS	Yield strength
ΔK	Stress-intensity range
ΔK_h	Overall stress-intensity range of a spectrum
ΔP	Load range
ΔP_h	Overall load range of a spectrum
$\Delta\sigma$	Stress range: Algebraic difference between successive valley and peak (positive or increasing) or between successive peak and valley (negative or decreasing)
$\Delta\sigma h$	Overall stress range in a spectrum
σ	Applied stress
$\sigma hmax$	Stress at largest (highest) peak of spectrum
$\sigma hmin$	Stress at smallest (lowest) valley of a spectrum
σsm	Spectrum mean stress

1. INTRODUCTION

Fatigue crack growth behavior under variable-amplitude loading is increasingly being used in the selection of materials for aircraft structures and their design, particularly for fatigue-critical structures. This is supplanting the selection of materials based on constant-amplitude fatigue crack growth resistance because the life of an aircraft structure cannot be predicted reliably using constant-amplitude fatigue crack growth data and existing life prediction techniques. Research in the last decade[1-12] has shown that load sequences have a considerable effect on fatigue crack propagation (FCP) behavior. In particular, the application of overloads or a few cycles at high tensile loads may cause retardation, that is, a temporary decrease in fatigue crack growth rate during subsequent lower amplitude cycles. Most of the work in the last decade was focused on understanding the effects of single overloads on fatigue crack growth rates.[1-10] Recently more emphasis is being placed upon the evaluation of fatigue crack growth under complex spectrum loading[11-14] simulating the loading experienced by aircraft structures.

The nature of a spectrum can vary widely depending on a particular component and type of aircraft. Depending on the specific details of load spectrums, FCP resistance for a given material also can vary widely. The reasons for differences in FCP resistance for the same material in different spectrums are generally unknown, since the load spectrums are complex and the interactions between alloy microstructure and variable-amplitude load histories are not well understood.

Research in the last decade[1-4,15-19] on high-strength aluminum alloys has identified several metallurgical factors which influence FCP resistance for constant-amplitude loading: alloy purity (Fe, Si content), temper, alloy content (e.g., Cu content), and dispersoid type (e.g., $Al_{12}Mg_2Cr$ in 7075 vs. Al_3Zr in 7050). However, the influence of these microstructural features on crack growth is not the same at intermediate and high growth rates, $>10^{-8}$ m/cycle (4×10^{-7} in./cycle) as it is at near-threshold rates, $<10^{-8}$ m/cycle. For example, overaging from a T6 temper to a T7 temper reduces FCP rates by a factor of two at intermediate stress intensities (ΔK) but can increase crack growth rates by a factor of ten at low ΔK. These studies demonstrate that different microstructural features control constant-amplitude FCP behavior at different ΔK values. Details of these microstructural/FCP behavior relationships will be addressed in Subsection 3.6 of this report.

The same level of understanding regarding microstructural effects on FCP under variable-amplitude loading does not exist. Whereas constant-amplitude loading characterizes the steady state FCP response of an alloy, FCP under variable-amplitude loading includes transient material responses not present in constant-amplitude FCP. Therefore, the understanding of microstructural effects on constant-amplitude FCP behavior is not sufficient to rationalize spectrum fatigue performance. In particular, the ability of an alloy to retard crack growth following a tensile overload is an important transient characteristic for assessing FCP life. However, since the present knowledge regarding the effect of microstructure on the retardation behavior of aluminum alloys is limited to studies involving simple overload spectrums, the results under complex spectrum loading at present cannot be understood.

Several mechanisms have been proposed to explain the observed retardation behavior following simple overloads. These include residual compressive stresses at the crack tip,[20,21] crack closure,[22-24] changes in the crack-tip plastic zone size,[1,20,25] crack blunting,[1,26] or combinations of these. A number of empirical models, based on either the crack closure[22,23] or plastic zone size[20,21] concepts, have been proposed that quantitatively take retardation into account in predicting FCP behavior. These models achieve satisfactory results only under certain specified conditions. However, when the test conditions are changed or broadened to include additional variables such as those existing in real spectrums, the models usually fail to predict observed crack growth lives.

The major weakness of all of these models is that they do not take into account either the metallurgical or the environmental factors that influence FCP. For instance, the Willenborg model predicts that materials with the same yield strength will exhibit similar retardation behavior.[20] Chanani[1] found that this was not the case for 2024-T8 and 7075-T73 heat treated to the same yield strength. He concluded that metallurgical variables such as precipitate morphology, dislocation interactions, and cyclic hardening exponent, have to be taken into account to explain the differences between the crack growth rates. Sanders, et al.,[2] had identified microstructural features such as precipitate morphology, intermetallic constituent particles, and dispersoid size as influencing FCP. Improved analytical life prediction capabilities would result if microstructure/load history interactions for spectrum FCP are understood and incorporated in such models.

The objectives of the multiphase NAVAIR program (N00019-80-C-0427,[27] N00019-81-C-0550,[28] and N00019-82-C-0425) are to perform a detailed metallurgical investigation of fatigue behavior and to simplify complex load histories. These spectrums will be representative of certain classes of applications and will provide information for development of fatigue-resistant alloys. As a major part of this effort, attention will be given to identifying metallurgical factors in high-strength aluminum alloys which control FCP behavior under spectrum loading. This knowledge of load history/microstructure interactions is essential to the development of criteria by which complex load histories can be standardized and simplified for materials evaluation.

The development of standardized and/or simplified load spectrums offers several advantages in characterizing the fatigue performance of engineering materials and designing fatigue resistant alloys. It is presently not cost-effective to develop alloys for high resistance to FCP under spectrum loading, since a wide variety of load histories must be considered. If a small number of standardized spectrums existed, more meaningful tests which consider spectrum loading could be included in alloy development/selection programs. Standardized load spectrums also would provide a common data base for comparisons of fatigue performance among various materials. The two spectrums in the program were simplified by eliminating half of the cycles and by eliminating the compression cycles. Selected existing life prediction tools were evaluated, and the potential of incorporating metallurgical factors in these models were examined.

This report describes the work completed in Phase III of this program and includes pertinent results from Phases I[27] and II[28] for completeness. Twelve commercial 2XXX and 7XXX aluminum alloys (Figure 1) were chosen for analysis so that the influence of both purity and temper on FCP could be evaluated. In Phases I and II, 10 of the alloys were evaluated; and in Phase III, two additional alloys were evaluated. The results on the 12 commercial 2XXX and 7XXX aluminum alloys are presented in Volume I of this report. The 12 alloys have been characterized with respect to chemical composition, microstructure, tensile properties, and fracture toughness. FCP tests were conducted on specimens of each of the 12 alloys for both constant-amplitude loading (including the low ΔK region) and two F-18 load spectrums. One F-18 load spectrum is a tension-dominated spectrum representing the lower wing root load history, and the other is a tension-compression spectrum representing the horizontal tail hinge moment load history. In the spectrum testing, one primary stress level was used for FCGR testing, while two other stress levels were used to obtain data at the low and high ends of the crack growth range. Fractographic examination of the spectrum fatigue specimens was used to document pertinent fracture features for each alloy. Six Al-Li alloys with systematically controlled microstructures were also evaluated in this program and the results are described in Volume II of this report.

The results of the tests performed using modified spectrums are also described in this report. Two different types of modifications were performed independently on the baseline spectrums. One modification had two goals: (1) to eliminate low-amplitude cycles to reduce testing time without changing the ranking (relative life) of the alloys, and (2) to determine the importance of low-amplitude cycles on the overall spectrum life. The second modification was made to determine the importance of compression cycles. Eight alloys (marked with + in Figure 1) were chosen for spectrum fatigue testing using the modified spectrums. These eight alloys were chosen from the 2XXX and 7XXX aluminum alloys so that the influences of purity, temper, and different alloy approaches were represented.

This report is written as an addendum to the Phase II Report.[28] In this phase two alloys were added to the original ten. The two alloys added were 2124-T351 and 7150-T6E189. The ten alloys previously evaluated were

INVESTIGATION OF FATIGUE CRACK GROWTH OF ALUMINUM ALLOYS UNDER SPECTRUM LOADING

MATERIALS

PREVIOUS PROGRAMS*

2020-T651 +
2024-T351 +
2024-T851 +
2124-T851
2324-T39
7050-T7451 +
7075-T651 +
7075-T7351 +
7475-T651 +
7475-T7351 +

CURRENT PROGRAM**

2124-T351
7150-T6E189

SPECIAL HEATS WITH SELECTED MICROSTRUCTURES***

SPECIFIC COMPARISONS

- ALLOY PURITY (FRACTURE TOUGHNESS)
  7075 vs 7475 and 2024 vs 2124
- PRECIPITATE STRUCTURE (TEMPER)
  2024-T351 vs T851, 2124-T351 vs T851, 7075-T651 vs T7351, and 7475-T651 vs T7351
- GRAIN SIZE
  RST (FINE) vs I/M (COARSE)**** and SYSTEMATICALLY CONTROLLED MICROSTRUCTURES***
- EXISTING ALLOYS vs NEW ALLOYS and APPROACHES
  7XXX vs CW67 RST**** and 7150, and 2XXX vs 2324 and Al-Li (SYSTEMATICALLY CONTROLLED MICROSTRUCTURES)***

GENERAL COMPARISONS

- MICROSTRUCTURE
- TENSILE
- FRACTURE TOUGHNESS
- CONSTANT-AMPLITUDE FATIGUE-CRACK GROWTH

LOAD HISTORY

- TWO F-18 SPECTRA (TENSION-DOMINATED and TENSION-COMPRESSION)
- THREE STRESS LEVELS
- MODIFICATIONS OF THE F-18 SPECTRUMS
- CRITICAL EXPERIMENTS****

SPECTRUM TEST SPECIMEN

- CENTER CRACKED PANEL – 6 mm THICK X 100 mm WIDE
- L-T ORIENTATION

SPECTRUM LIFE PREDICTIONS**

*PREVIOUS PROGRAMS, CONTRACT NOS. N00019-80-C-0427 and N00019-81-C-0550
**CURRENT PROGRAM, CONTRACT NO. N00019-82-C-0425
***CURRENT PROGRAM, SEPARATE REPORT
****FUTURE PLANNED EFFORT
+MATERIALS TESTED WITH MODIFIED SPECTRUMS

FIGURE 1. PROGRAM OUTLINE

2020-T651, 2024-T351, 2024-T851, 2124-T851, 2324-T39, 7050-T7451, 7075-T651, 7075-T7351, 7475-T651, and 7475-T7351.

In this report the new data are given in detail and most figures and tables from the Phase II report[28] are updated to include the new information. A limited number of copies of that report are available on request. A summary of that work is also published in "Advances in Fracture Research – Proceedings of the Sixth International Conference on Fracture."[30,31]

2. EXPERIMENTAL PROCEDURE

All procedures and spectrums were identical to those used in Phase II and described in Reference 28. Note that the designation of 7050-T73651 has been changed to 7050-T7451 to reflect the change made by the Aluminum Association.

3. RESULTS AND DISCUSSION

The results for 2124-T351 and 7150-T6E189 are presented with summaries for all 12 alloys. Discussion is primarily limited to differences in results from those found in Phase II.

3.1 CHEMISTRY

The chemical composition of all 12 alloys are listed in Table 1 along with the commercial limits for each. All 12 alloys are within the appropriate composition limits.

3.2 MICROSTRUCTURAL EVALUATION

Alloys 2124-T351 and 7150-T6E189 are variants of commercial alloys examined in Phases I and II of this contract; as such, there are few microstructural distinctions between these two alloys and those studied previously. Alloy 2124-T351 is a high-purity, naturally aged variant of 2024. The as-polished microstructure (Figure 2a) indicates the distribution of constituent phases, which include insoluble $Al_{12}(Fe,Mn)_3Si$ and Al_7Cu_2Fe particles, and partially soluble Mg_2Si and Al_2CuMg phases. The volume fraction of these constituents is substantially lower than in 2024, owing to the lower Fe plus Si content in 2124. As is the case in other 2X24 alloys, the grain morphology is a coarse, recrystallized structure (Figure 2b).

Alloy 7150 is a minor compositional variant of 7050 developed jointly by Alcoa and Boeing for maximum strength. The T6E189 temper is an Alcoa-designed practice which provides improved exfoliation resistance over the original T651 temper without sacrificing either strength or SCC resistance. Like 2124, 7150 has low Fe plus Si content and relatively small volume fractions of constituents (Figure 3a). As for other 7XXX alloys, these constituents include Al_7Cu_2Fe, Mg_2Si, and Al_2CuMg. The grain structure of 7X50 alloys generally exhibits a low degree of recrystallization, as in Figure 3b; this

TABLE 1. CHEMICAL COMPOSITION OF PROGRAM MATERIALS

MATERIAL	SAMPLE NO.	ELEMENT, WEIGHT PERCENT										
		LIMITS	Cu	Mg	Zn	Mn	Cr	Ti	Be	Fe	Si	OTHER
2020-T651	523713-B		4.44	–	0.03	0.52		0.02		0.20	0.09	1.09Li 0.20Cd
2024-T351	511338		4.35	1.54	0.07	0.51	0.00	0.03	–	0.23	0.09	
-T851	511339		4.41	1.50	0.09	0.50	0.00	0.02	–	0.33	0.10	–
		MINIMUM	3.8	1.2	–	0.30	–	–	–	–	–	–
		MAXIMUM	4.9	1.8	0.25	0.9	0.10	0.15	–	0.50	0.50	–
2124-T351	554885		3.91	1.35	0.02	0.48	–	0.01	–	0.07	0.05	–
-T851	511340		4.21	1.46	0.03	0.47	0.00	0.01	–	0.10	0.05	–
		MINIMUM	3.8	1.2	–	0.30	–	–	–	–	–	–
		MAXIMUM	4.9	1.8	0.25	0.9	0.10	0.15	–	0.30	0.20	–
2324-T39	492513		4.23	1.52	0.01	0.51	0.00	0.01	0.002	0.08	0.05	–
		MINIMUM	3.8	1.2	–	0.3	–	–	–	–	–	–
		MAXIMUM	4.4	1.8	0.25	0.9	0.10	–	–	0.12	0.10	–
7075-T651	475332		1.70	2.41	5.62	0.05	0.20	0.06	0.002	0.26	0.12	–
-T7351	511341		1.95	2.63	5.79	0.04	0.18	0.04	–	0.27	0.09	–
		MINIMUM	1.2	2.1	5.1	–	0.18	–	–	–	–	–
		MAXIMUM	2.0	2.9	6.1	0.30	0.28	0.20	–	0.50	0.40	–
7050-T73651	511464		2.23	2.30	6.27	0.02	0.01	0.03	0.002	0.13	0.07	0.12Zr
		MINIMUM	2.0	1.9	5.7	–	–	–	–	–	–	0.08Zr
		MAXIMUM	2.6	2.6	6.7	0.10	0.04	0.06	0.05	0.15	0.12	0.15Zr
7150-T6E189	536031		2.09	2.23	6.29	0.01	0.00	0.04	–	0.11	0.05	–
		MINIMUM	1.9	2.0	5.9	–	–	–	–	–	–	–
		MAXIMUM	2.5	2.7	6.9	0.10	0.04	0.06	–	0.15	0.12	–
7475-T651	511463		1.48	2.36	5.46	0.00	0.21	0.02	0.002	0.07	0.04	–
-T7351	511630		1.6	2.43	5.67	0.00	0.17	0.02	0.001	0.06	0.05	–
		MINIMUM	1.2	1.9	5.2	–	0.18	–	–	–	–	–
		MAXIMUM	1.9	2.6	6.2	0.06	0.25	0.06	0.05	0.12	0.1	–

a. AS POLISHED 500x 85-02226

b. GRAFF/SARGENT + KELLERS 250x 85-02233

FIGURE 2. OPTICAL MICROGRAPHS OF ALLOY 2124-T351, LONGITUDINAL PLANE

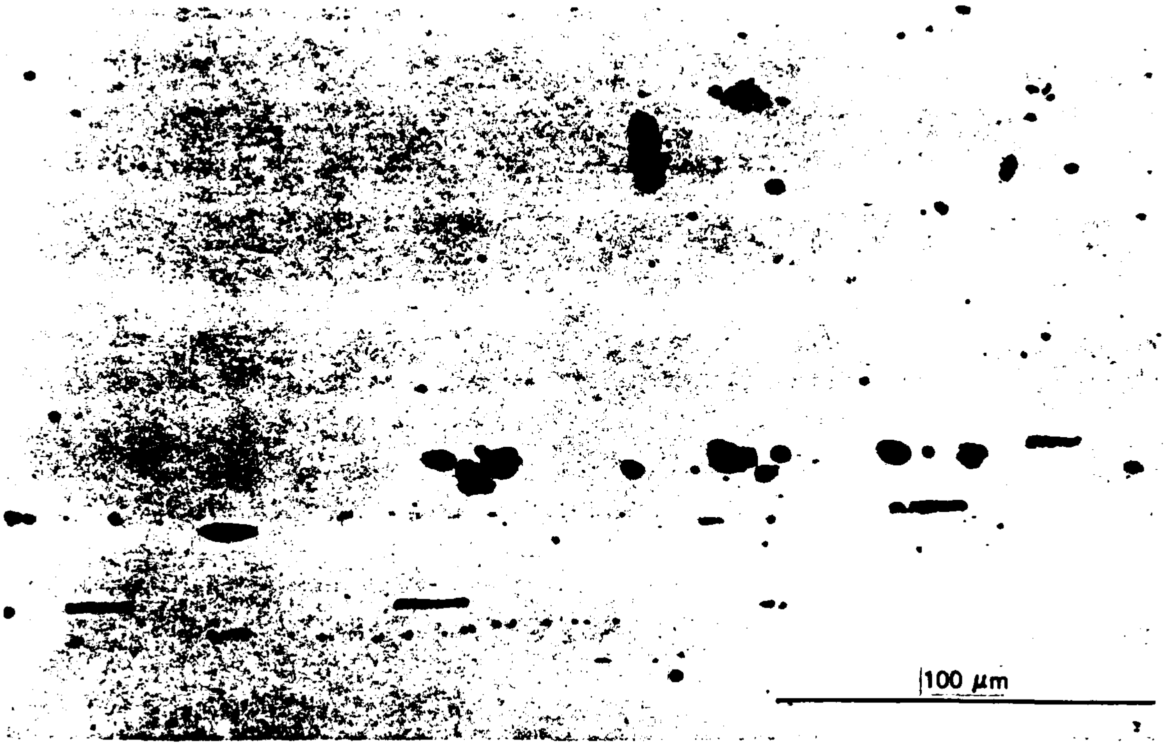

a. AS POLISHED 500x 85-02219-1

b. KELLER'S ETCH 250x 85-02219-2

FIGURE 3. OPTICAL MICROGRAPHS OF ALLOY 7150-T6E189, LONGITUDINAL PLANE

structure is maintained by Al_3Zr dispersoids, which are finely distributed throughout the microstructure and are too small to be seen optically.

The fine microstructural features (optically unresolvable) of 2124-T351 and 7150-T6E189 are analogous, respectively, to those of 2124-T351 and 7050-T7451; these were discussed in the previous reports.[27, 28]

3.3 TENSILE AND FRACTURE TOUGHNESS RESULTS

The tensile and fracture toughness results for 2124-T351 and 7150-T6E189 are given in Tables 2 and 3. Alloy 7150-T6E189 is the strongest alloy evaluated in the program with both the highest ultimate and yield strengths. The 12 alloys are compared in Figure 4. Note that the toughness value for 2124-T351 is not valid per ASTM E399 nor meaningful per ASTM B646.

3.4 FATIGUE CRACK GROWTH RESULTS UNDER CONSTANT-AMPLITUDE LOADING

Fatigue crack growth data were generated for all alloys from near-threshold (ΔK_{th}) through intermediate ΔK values, with measured near-threshold FCG rates approaching 10^{-10} m/cycle (4 x 10^{-9} in./cycle). The FCGR data for the two alloys evaluated in this phase are presented in Figures A-1 and A-2 in Appendix A. In Figure 5, the da/dN versus ΔK curves for all 12 alloys are shown. In addition, the FCGR data are shown in Figure 6 and Table 4 as the stress intensity required to drive a fatigue crack at a specified rate. In Figure 6 the results are grouped into 2000 and 7000 series and, within the groups, are in descending order of their spectrum fatigue lives (Subsection 3.5).

3.5 SPECTRUM TEST RESULTS

The spectrum life results for each test are presented in Table 5. Overall, the results were reproducible, with the maximum difference between the lives of duplicate tests being 22 percent. Crack length versus simulated flight hour data (a versus H) are shown graphically in Appendix B, while results for spectrum crack growth rate versus maximum peak stress intensity (da/dH versus K_{hmax}) are shown in Appendix C. For comparison, spectrum crack growth rate curves (da/dH versus K_{hmax}) for all 12 materials are

TABLE 2. TENSILE RESULTS – LONGITUDINAL

MATERIAL PLATE THICKNESS mm (in.)	SPECIMEN LOCATION[ab]	ULTIMATE STRENGTH MPa (ksi)	YIELD STRENGTH MPa (ksi)	ELONGATION IN 4D %[b]	REDUCTION OF AREA %[b]
2124-T351	T/4	471(68)	370(54)	23	26
25.4(1.0)	T/2	462(67)	359(52)	22	26
	T/2	462(67)	358(52)	23	30
	3T/4	469(68)	369(54)	23	25
	AVERAGE	466(68)	364(53)	22	27
	AVG T/4, 3T/4	470(68)	369(54)	23	26
7150-T6E189	T/4	631(91)	585(85)	12	22
25.4 (1.0)	T/2	628(91)	581(84)	11	18
	T/2	628(91)	581(84)	11	18
	3T/4	635(92)	585(85)	12	18
	AVERAGE	631(91)	584(85)	12	20
	AVG T/4, 3T/4	633(92)	585(85)	12	20

a SPECIMENS TAKEN FROM THE T/2 LOCATION ARE FROM THE CENTER OF THE PLATE THICKNESS AND THOSE FROM THE T/4 AND 3T/4 ARE FROM MIDWAY BETWEEN THE CENTER AND THE TOP SURFACE OR BOTTOM SURFACE, RESPECTIVELY

b THE NOMINAL DIAMETER OF THE REDUCED-SECTION OF T/2 SPECIMENS WAS 12.7MM AND T/4 AND 3T/4 SPECIMENS WAS 6.4MM

TABLE 3. FRACTURE TOUGHNESS RESULTS, L-T ORIENTATION

ALLOY AND TEMPER	PLATE THICKNESS mm (in.)	SPECIMEN THICKNESS mm	K_Q MPa $\sqrt{m}$ (ksi $\sqrt{in.}$)	VALID K_{IC} PER ASTM E399	AVERAGE VALID K_{IC} OR MEANINGFUL K_Q MPa $\sqrt{m}$ (ksi $\sqrt{in.}$)
2124-T351	25.4(1.0)	25.4	50(46)	NO[a]	–
			45(41)	NO[a]	–
7150-T6E189	25.4(1.0)	25.4	30(27)	YES	31(28)
			32(29)	YES	

a TEST INVALID PER ASTM E399 DUE TO INSUFFICIENT THICKNESS AND FATIGUE CRACK LENGTH, AND $P_{MAX}/P_Q > 1.10$

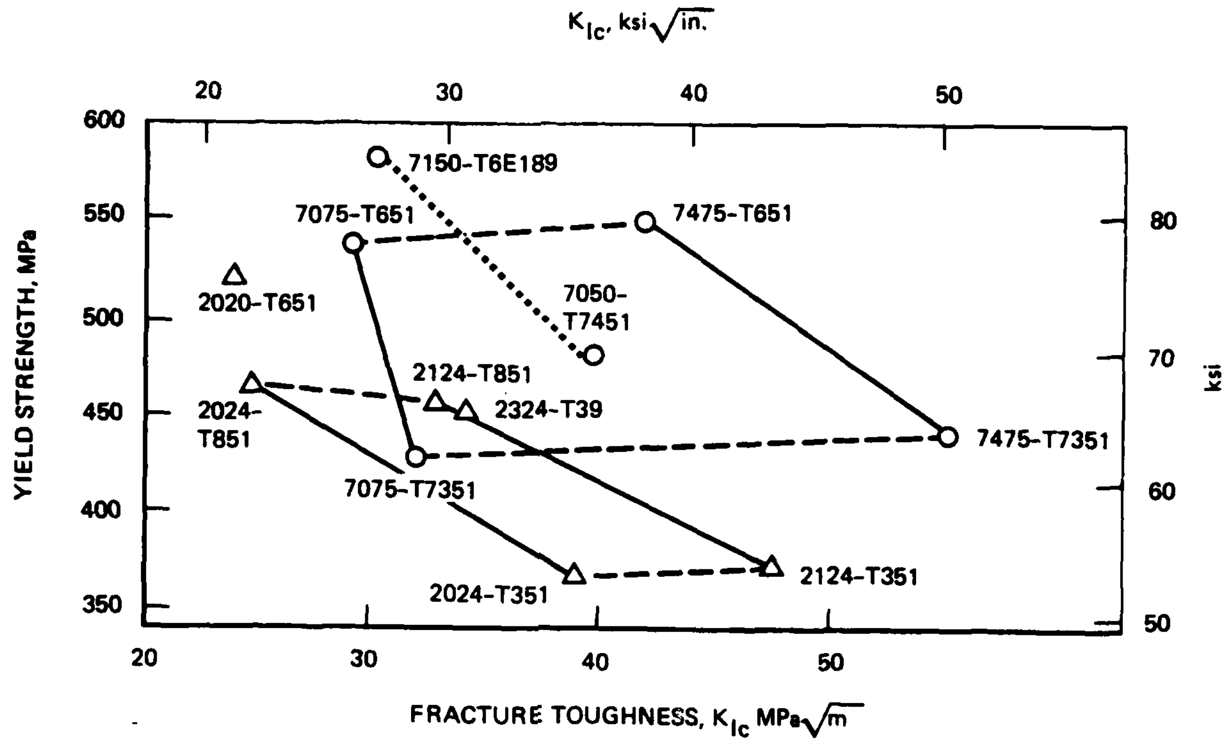

FIGURE 4. RELATIONSHIP BETWEEN YIELD STRENGTH AND FRACTURE TOUGHNESS

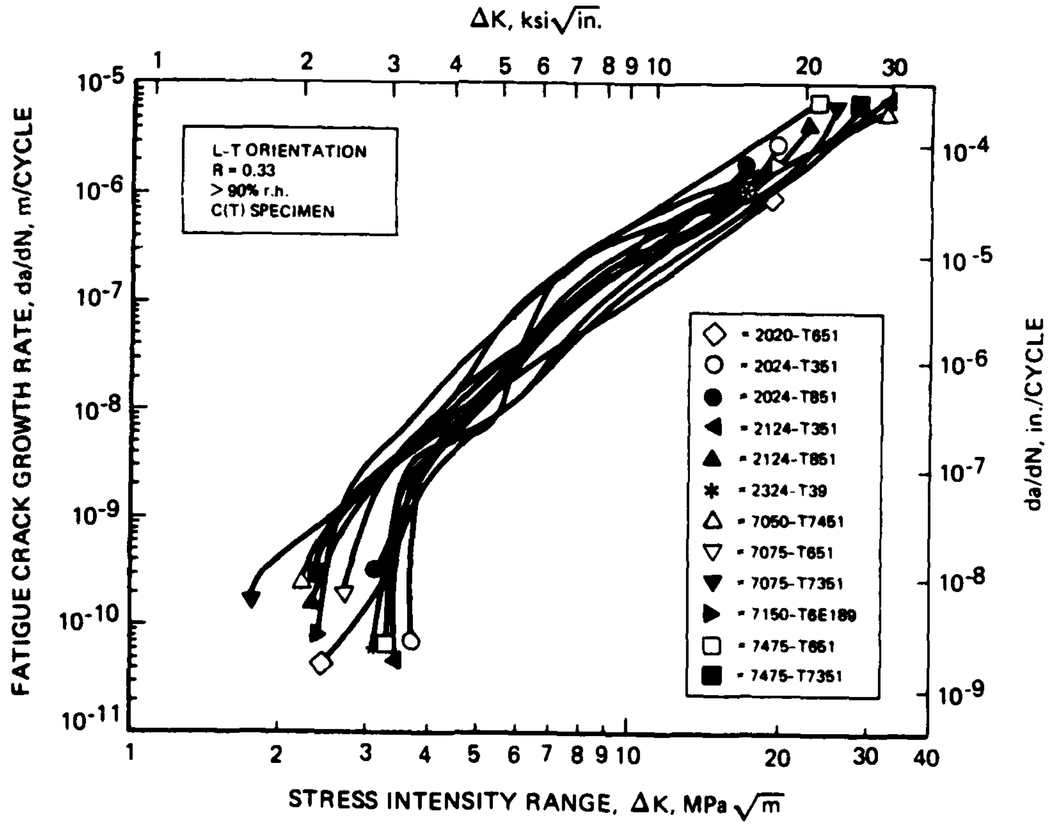

FIGURE 5. CONSTANT AMPLITUDE FCGR CURVES

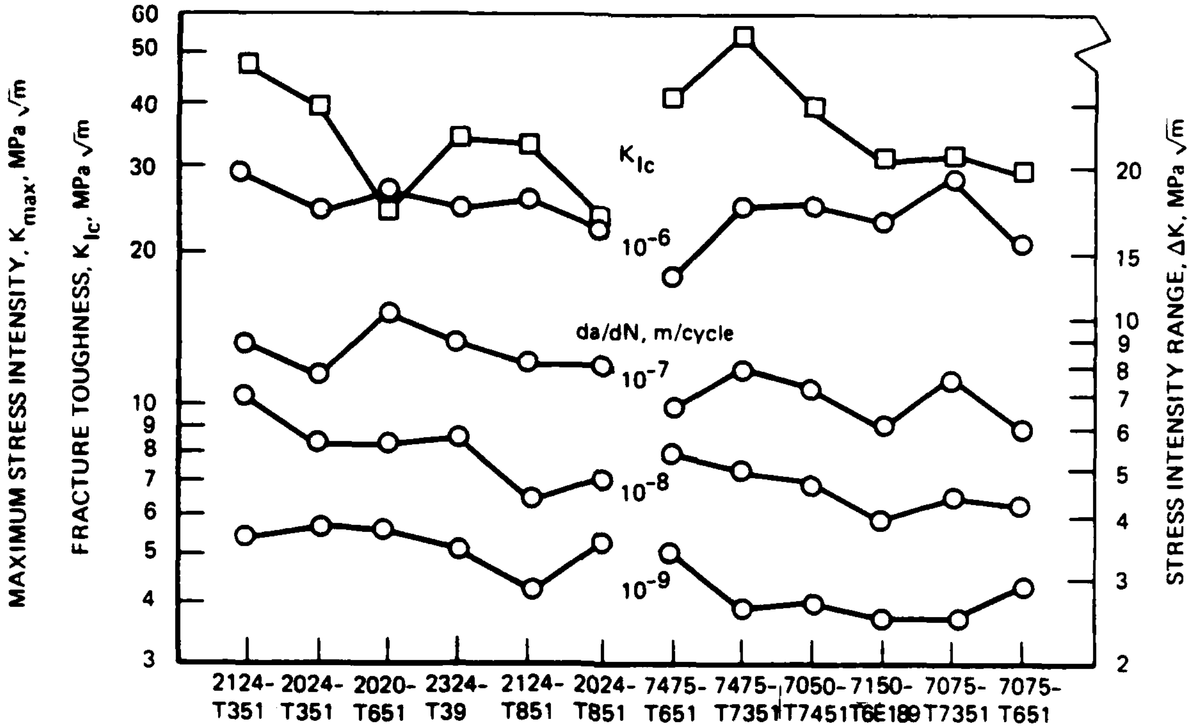

FIGURE 6. STRESS INTENSITY NEEDED TO OBTAIN A GIVEN FATIGUE CRACK GROWTH RATE UNDER CONSTANT-AMPLITUDE LOADING. (R = 0.33, > 90% rh, L-T ORIENTATION)

TABLE 4. RANKING OF MATERIALS BY STRESS INTENSITY RANGE TO OBTAIN A GIVEN FATIGUE CRACK GROWTH RATE UNDER CONSTANT-AMPLITUDE LOADING

	ΔK, MPA $\sqrt{m}$ (ksi $\sqrt{in.}$) TO OBTAIN A GIVEN FCGR									
FCGR	RANK	10^{-10} m/CYCLE (4×10^{-9} in/CYCLE)	RANK	10^{-9} M/CYCLE (4×10^{-8} in/CYCLE)	RANK	10^{-8} m/CYCLE (4×10^{-7} in/CYCLE)	RANK	10^{-7} m/CYCLE (4×10^{-6} in/CYCLE)	RANK	10^{-6} m/CYCLE (4×10^{-5} in/CYCLE)
MATERIAL										
2020-T651	5	2.9 (2.7)	2	3.7 (3.4)	3	5.5 (5.0)	1	10.2 (9.3)	3	18.0 (16.4)
2024-T351	1	3.7 (3.4)	1	3.8 (3.5)	3	5.5 (5.0)	7	7.6 (6.9)	8	16.2 (14.7)
2024-T851	6	2.7 (2.5)[a]	4	3.5 (3.2)	7	4.8 (4.4)	4	8.0 (7.3)	10	15.0 (13.7)
2124-T351	2	3.5 (3.2)	3	3.6 (3.3)	1	6.8 (6.2)	3	8.8 (8.0)	1	19.1 (17.4)
2124-T851	9	2.2 (2.0)[a]	8	2.8 (2.5)	10	4.3 (3.9)	4	8.0 (7.3)	4	17.2 (15.7)
2324-T39	4	3.2 (2.9)	6	3.4 (3.1)	2	5.7 (5.2)	2	8.9 (8.1)	7	16.4 (14.9)
7050-T73651	10	2.1 (1.9)[a]	9	2.7 (2.5)	8	4.7 (4.3)	8	7.2 (6.6)	5	16.9 (15.4)
7075-T651	7	2.6 (2.3)[a]	7	2.9 (2.7)	11	4.2 (3.9)	11	6.0 (5.5)	11	14.0 (12.7)
7075-T7351	12	1.7 (1.6)[a]	11	2.5 (2.3)	9	4.4 (4.0)	7	7.6 (6.9)	2	19.0 (17.3)
7150-T6E189	8	2.4 (2.2)	11	2.5 (2.3)	12	3.9 (3.5)	11	6.0 (5.5)	9	15.5 (14.1)
7475-T651	3	3.3 (3.0)	5	3.4 (3.1)	5	5.4 (4.9)	10	6.6 (6.0)	12	12.1 (11.0)
7475-T7351	11	2.0 (1.8)[a]	10	2.6 (2.4)	6	4.9 (4.5)	4	8.0 (7.3)	6	16.6 (15.1)

a EXTRAPOLATED

TABLE 5. SPECTRUM FATIGUE RESULTS – BASELINE SPECTRUMS

MAXIMUM PEAK STRESS σ_{hmax}	SIMULATED FLIGHT HOURS, H					
	103 MPa (15 ksi)		145 MPa (21 ksi)		169 MPa (24.5 ksi)	
SPECTRUM	TD	TC	TD	TC	TD	TC
CRACK-GROWTH REGIME, a_i to a_f	6-13 mm 0.24-0.51 in.	6-13 mm 0.24-0.51 in.	6 mm-F[a] 0.24 in.-F	6 mm-F 0.24 in.-F	18 mm-F 0.71 in.-F	18 mm-F 0.71 in.-F
MATERIAL[b]						
2020-T651	78,416	54,895	17,188	14,575	0[c]	0[c]
	–	–	20,020	11,717	–	–
2024-T351	26,412	24,633	21,719	15,375	2,451	1,092
	28,027	24,035	22,565	15,389	2,363	1,192
			22,122			
2024-T851	18,297	18,299	8,505	7,031	196	0[c]
	19,258	17,824	8,557	7,132	184	0[c]
2124-T351	33,132	25,536	25,642	18,800	4,329	2,165
	–	–	25,459	19,664	–	–
2124-T851	17,274	15,787	11,244	8,853	851	1,085
	16,769	15,563	11,096	9,314	828	1,245
2324-T39	29,057	24,616	18,148	15,338	2,443	1,159
	–	–	17,547	13,529	–	–
7050-T7451	18,741	19,467	14,496	13,340	2,260	1,638
	18,930	16,217	15,223	12,962	2,455	1,837
7075-T651	14,775	13,886	9,820	8,617	651	380
	–	–	11,945	9,181	–	–
7075-T7351	17,642	16,666	13,517	10,392	1,300	740
	16,910	16,529	12,314	10,934	1,601	781
7150-T6E189	13,299	13,329	12,857	11,179	1,079	585
	–	–	13,234	11,574	–	–
7475-T651	15,387	15,522	18,303	14,744	3,777	2,661
	15,384	16,624	19,792	15,141	3,197	2,608
7475-T7351	18,241	16,578	15,417	13,410	2,714	2,152
	18,873	17,332	14,661	13,345	2,852	2,256

a F = FAILURE

b RESULTS FOR 2124-T351 AND 7150-T6E189 ARE FOR PRESENT EFFORT, OTHER RESULTS FROM PHASES I AND II

c SPECIMEN FRACTURED BEFORE REACHING INITIAL CRACK LENGTH, a_i, OF 18mm, FOR THESE 169 MPa (24.5 ksi) TESTS, IN FATIGUE shown in Figure 7. For easier comparison of resistance to spectrum crack growth among all 12 materials for both spectrums, the maximum peak stress intensities to obtain a given crack-growth rate are shown in Figure 8 and Table 6 in presentations similar to those for the constant-amplitude data in Figure 6 and Table 4.

The alloys are ranked by their spectrum fatigue lives for each spectrum (average of the two duplicate tests) in Table 7 and in Figure 9.

The relationship between spectrum fatigue lives and yield strength and fracture toughness is shown in Figures 10 and 11, respectively.

All alloys were evaluated at two other maximum peak stresses, 103 MPa (15 ksi) and 169 MPa (24.5 ksi). As described in the Phase II report,[28] two test procedures were used. Results are presented in Table 8 and Figure 12 for the five alloys evaluated in Phases II and III from a crack length of 6 mm to failure.

The spectrum fatigue results for 7475-T651 were unusual in comparison to the other alloys. The notable differences were that (1) the life for the 7475-T651 with lower toughness was longer than for 7475-T351, and (2) that the spectrum FCG rates were faster than all other alloys at the lowest maximum peak stress intensities (Figure 7) and were slower at the higher maximum peak stress intensities. To evaluate a second lot of material was beyond the scope of the program. Therefore, at their own expense, Northrop and Alcoa evaluated a second lot of 7475-T651 to determine whether this behavior was repeatable. The results and discussion of this evaluation are presented in Appendix E. The behavior of the second lot confirmed the results for the first lot evaluated in Phase I.

3.6 FRACTOGRAPHIC EXAMINATION OF SPECTRUM FATIGUE SPECIMENS

As noted in Subsection 3.2, the microstructures of 2124-T351 and 7150-T6E189 are similar to those of 2024-T351 and 7050-T7451, respectively. The spectrum fatigue data also show a great deal of similarity between 2024 and 2124, and between 7050 and 7150. It would be expected, therefore, that the fatigue fracture surfaces for these pairs of alloys should be similar as well; this is, in fact, what is observed. As has been done in Phases I and II, the specimens were examined primarily at crack lengths of 6 and 19 mm (0.25 and

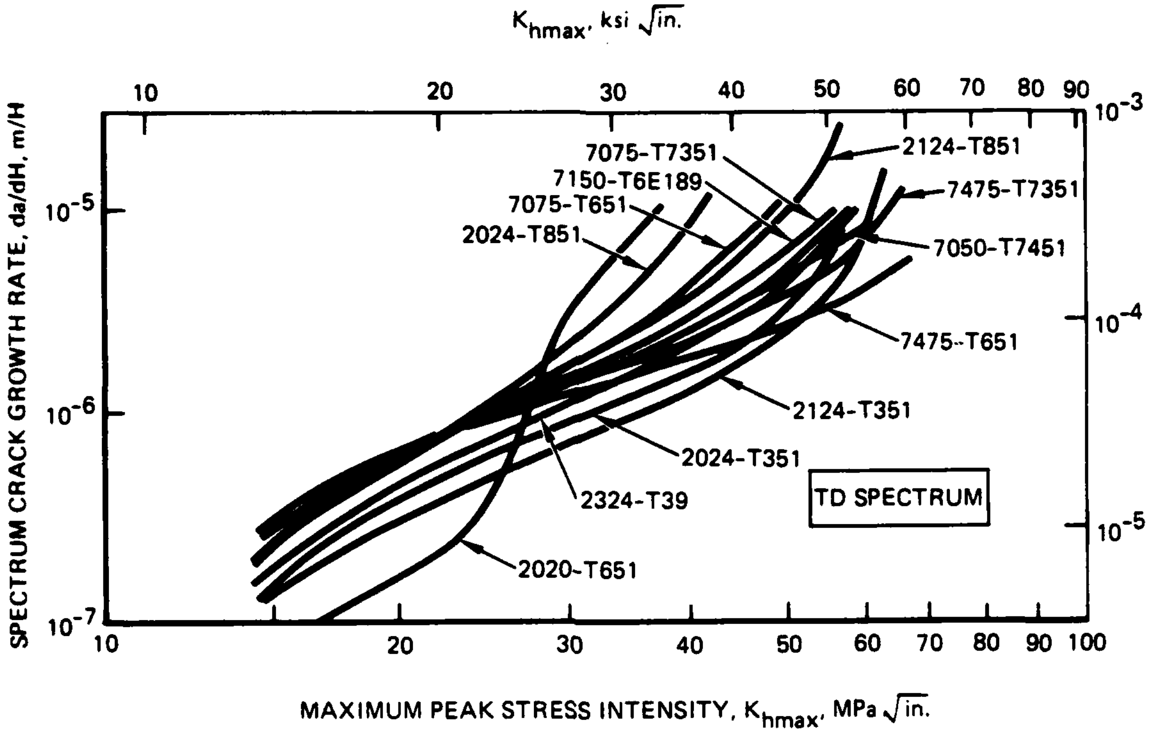

FIGURE 7. SPECTRUM FCGR CURVES FOR TD SPECTRUM

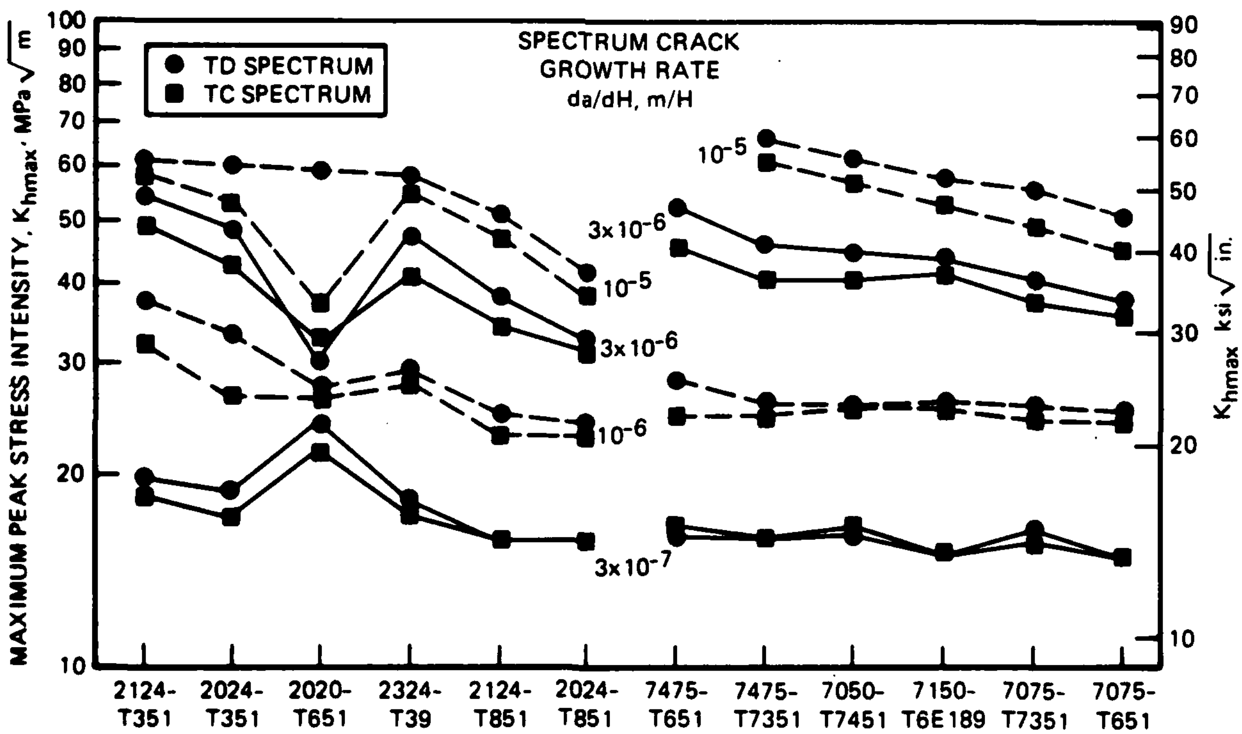

FIGURE 8. MAXIMUM PEAK STRESS INTENSITY NEEDED TO OBTAIN A GIVEN SPECTRUM FCGR FOR TD AND TC SPECTRUMS

TABLE 6. RANKING OF MATERIALS IN SPECTRUM FATIGUE BY MAXIMUM PEAK STRESS INTENSITY TO OBTAIN A GIVEN FATIGUE CRACK GROWTH RATE

	K_{hmax}, MPa $\sqrt{m}$ (ksi $\sqrt{in.}$) TO OBTAIN A GIVEN SPECTRUM FCGR											
FCGR	3×10^{-7} m/H[a] (1.2×10^{-5} in./H)			10^{-6} m/H (4×10^{-5} in./H)[b]			3×10^{-6} m/H (1.2×10^{-4} in./H)[c]			10^{-5} m/H (4×10^{-4} in./H)[d]		
SPECTRUM	TD	RANK[e]	TC	TD	RANK[e]	TC	TD	RANK[e]	TC	TD	RANK[e]	TC
MATERIAL												
2020-T651	24.1 (21.9)	1	21.9 (19.9)	27.1 (24.9)	4	26.3 (23.9)	30 (28)	11	32 (29)	37 (34)	11	37 (34)
2024-T351	18.8 (17.1)	3	17.0 (15.5)	33.0 (30.0)	2	26.5 (24.1)	48 (44)	3	42 (38)	– –	5	53 (48)
2024-T851	16.0 (14.6)	9	15.9 (14.5)	24.0 (21.8)	12	23.0 (20.9)	32 (29)	11	31 (28)	41 (37)	10	38 (35)
2124-T351	19.8 (18.0)	2	18.4 (16.7)	37.0 (33.7)	1	32.0 (29.1)	54 (49)	1	49 (45)	61 (56)	3	58 (53)
2124-T851	15.8 (14.4)	10	15.7 (14.3)	24.8 (22.6)	11	23.0 (20.9)	38 (35)	9	34 (31)	51 (46)	8	47 (43)
2324-T39	18.1 (16.5)	4	17.5 (15.9)	29.0 (26.4)	3	28.1 (25.6)	47 (43)	4	41 (37)	58 (53)	2	55 (50)
7050-T73651	16.2 (14.7)	5	16.5 (15.0)	25.5 (23.2)	6	25.5 (23.2)	44 (40)	6	40 (36)	– –	4	57 (52)
7075-T651	14.8 (13.5)	12	14.8 (13.5)	24.9 (22.7)	10	23.8 (21.7)	37 (34)	10	35 (32)	50 (46)	9	44 (40)
7075-T7351	16.4 (14.9)	7	15.9 (14.5)	25.5 (23.2)	9	24.2 (22.0)	40 (36)	8	37 (34)	55 (50)	7	49 (45)
7150-T6E189	14.8 (13.5)	11	15.0 (13.7)	26.0 (23.7)	8	25.6 (23.3)	43 (39)	6	41 (37)	57 (52)	6	52 (47)
7475-T651	16.2 (14.7)	5	16.5 (15.0)	28.0 (25.5)	5	24.7 (22.5)	52 (47)	2	45 (41)	– –	1[f]	– –
7475-T7351	16.0 (14.7)	8	15.9 (14.5)	25.5 (23.2)	7	24.5 (22.3)	45 (41)	5	40 (36)	65 (59)	2	61 (56)

a σ_{hmax} = 103 MPa (15 ksi)
b σ_{hmax} = 103 MPa (15 ksi) and 145 MPa (21 ksi)
c σ_{hmax} = 145 MPa 21 ksi
d σ_{hmax} = 145 MPa (21 ksi) and 169 MPa (24.5 ksi)
e BASED ON AVERAGE TD AND TC SPECTRUM
f BASED ON EXTRAPOLATION

TABLE 7. RANKING OF MATERIALS UNDER SPECTRUM LOADING – BASELINE SPECTRUMS

AVERAGES OF TWO TESTS ROUNDED TO NEAREST HUNDRED HOURS

a. σ_{hmax} = 103 MPa FROM a = 6 TO 13 mm

TD SPECTRUM		TC SPECTRUM	
MATERIAL	SIMULATED FLIGHT HOURS	MATERIAL	SIMULATED FLIGHT HOURS
2020-T651	78,400[a]	2020-T651	54,900[a]
2124-T351	33,100[a]	2124-T351	25,500[a]
2324-T39	29,100[a]	2324-T39	24,600
2024-T351	27,200	2024-T351	24,300[a]
7050-T7451	18,800	2024-T851	18,100
2024-T851	18,800	7050-T7451	17,800
7475-T7351	18,600	7475-T7351	17,000
7075-T7351	17,300	7075-T7351	16,600
2124-T851	17,300	7475-T651	16,100
7475-T651	15,400	2124-T851	15,700
7075-T651	14,800[a]	7075-T651	13,900[a]
7150-T6E189	13,300[a]	7150-T6E189	13,300[a]

b. σ_{hmax} = 145 MPa FROM a = 6 mm TO FAILURE

TD SPECTRUM		TC SPECTRUM	
MATERIAL	SIMULATED FLIGHT HOURS	MATERIAL	SIMULATED FLIGHT HOURS
2124-T351	25,600	2124-T351	19,200
2024-T351	22,100	2024-T351	15,400
7475-T651	19,000	7475-T651	14,900
2020-T651	18,500	2324-T39	14,400
2324-T39	17,800	7475-T7351	13,400
7475-T7351	15,000	7050-T7451	13,200
7050-T7451	14,900	2020-T651	13,100
7150-T6E189	13,000	7150-T6E189	11,300
7075-T7351	12,900	7075-T7351	10,700
2124-T851	11,200	2124-T851	9,100
7075-T651	10,800	7075-T651	8,900
2024-T851	8,500	2024-T851	7,100

c. σ_{hmax} = 169 MPa FROM a = 18 mm TO FAILURE

TD SPECTRUM		TC SPECTRUM	
MATERIAL	SIMULATED FLIGHT HOURS	MATERIAL	SIMULATED FLIGHT HOURS
2124-7351	4,300[a]	7475-T651	2,600
7475-T651	3,400	7475-T7351	2,200
7475-T7351	2,800	2124-T351	2,200[a]
2324-T39	2,400[a]	7050-T7451	1,700
2024-T351	2,400	2124-T851	1,200
7050-T7451	2,400	2324-T39	1,200[a]
7075-T7351	1,400	2024-T351	1,100
7150-T6E189	1,100[a]	7075-T7351	800
2124-T851	800	7150-T6E189	600[a]
7075-T651	700[a]	7075-T651	400[a]
2024-T851	200	2024-T851	0[b]
2020-T651	0[ab]	2020-T651	0[ab]

a ONE TEST RESULT

b SPECIMEN FRACTURED BEFORE REACHING INITIAL CRACK LENGTH

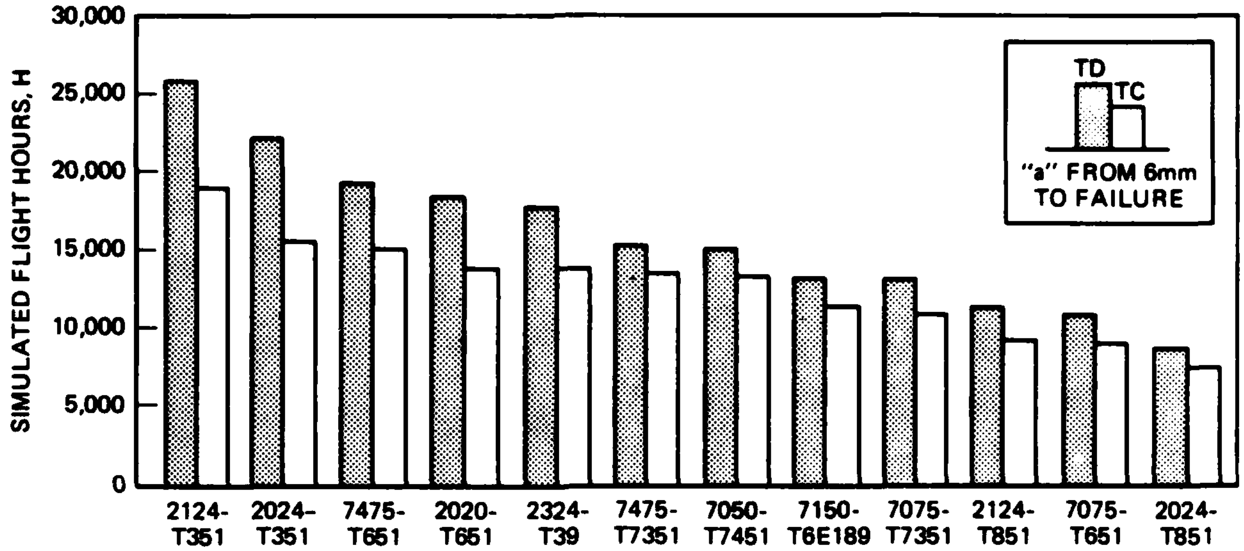

FIGURE 9. SPECTRUM FATIGUE LIVES AT 145 MPa (21 ksi)

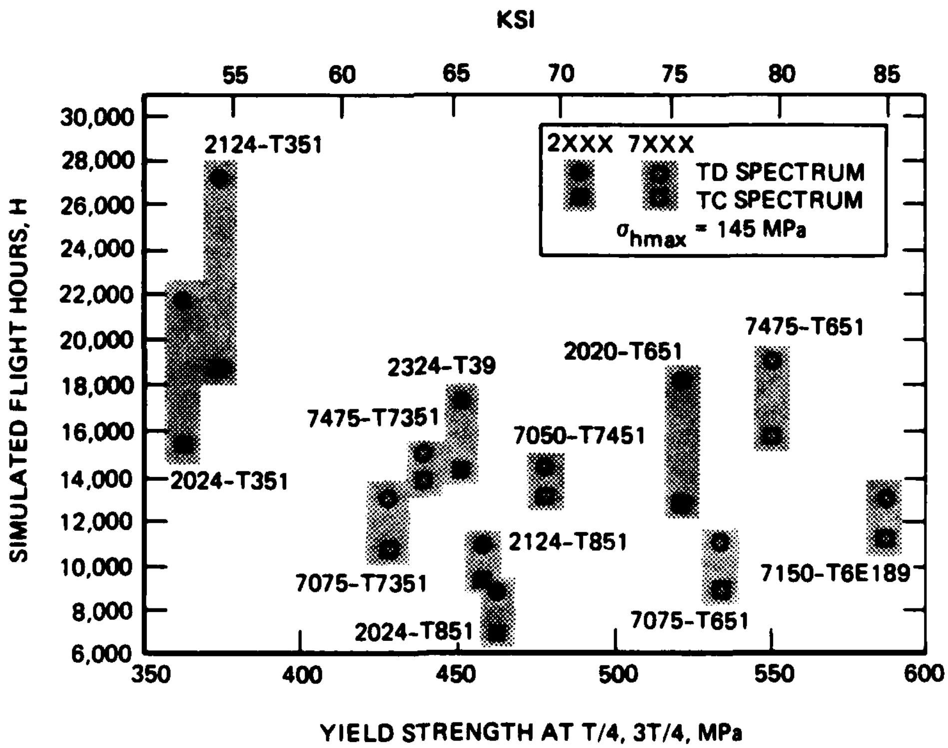

FIGURE 10. SPECTRUM LIFE VERSUS YIELD STRENGTH

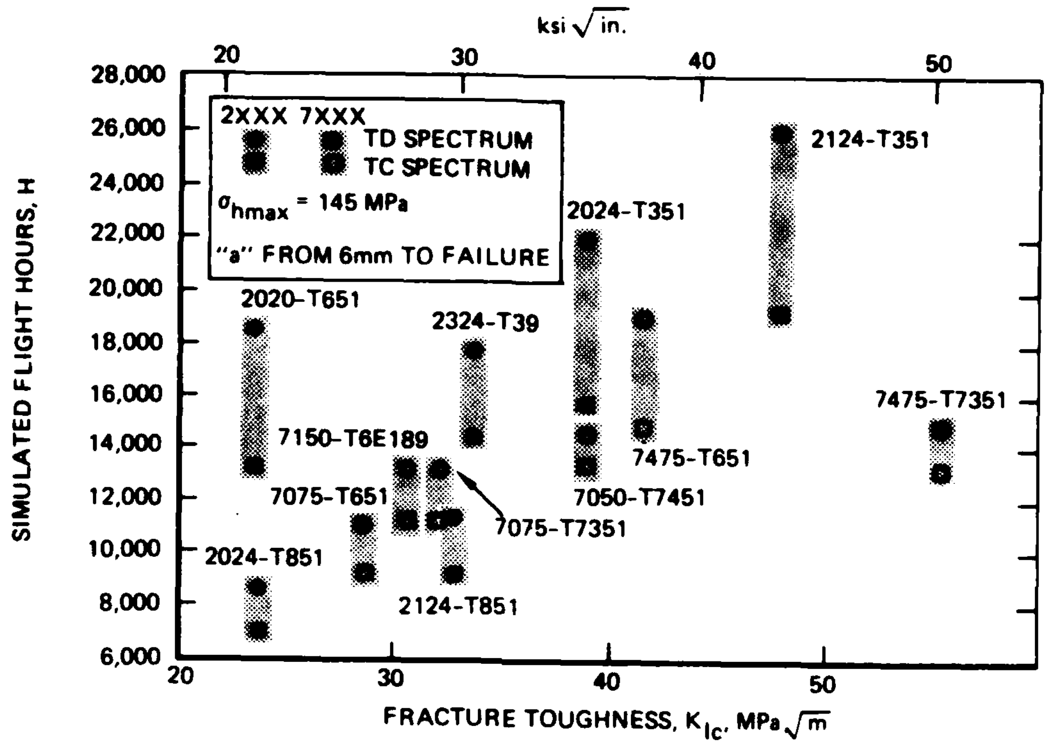

FIGURE 11. SPECTRUM LIFE VERSUS FRACTURE TOUGHNESS

TABLE 8. SPECTRUM FATIGUE LIVES AT 103 MPa AND 169 MPa FOR "a" FROM 6MM (0.24 IN.) TO FAILURE

MAXIMUM PEAK STRESS σ_{hmax}	SIMULATED FLIGHT HOURS, H			
	103 MPa (15 ksi)		169 MPa (24.5 ksi)	
SPECTRUM	TD	TC	TD	TC
MATERIAL				
2020-T651	83,910	80,953	6,217	3,636
2124-T351	64,275	50.607	17,530	11,662
2324-T39	53,738	42,939	11,862	8,261
7075-T651	27,341	25,268	6,333	4,612
7150-T6E189	21,281	27,760	7,349	7,520

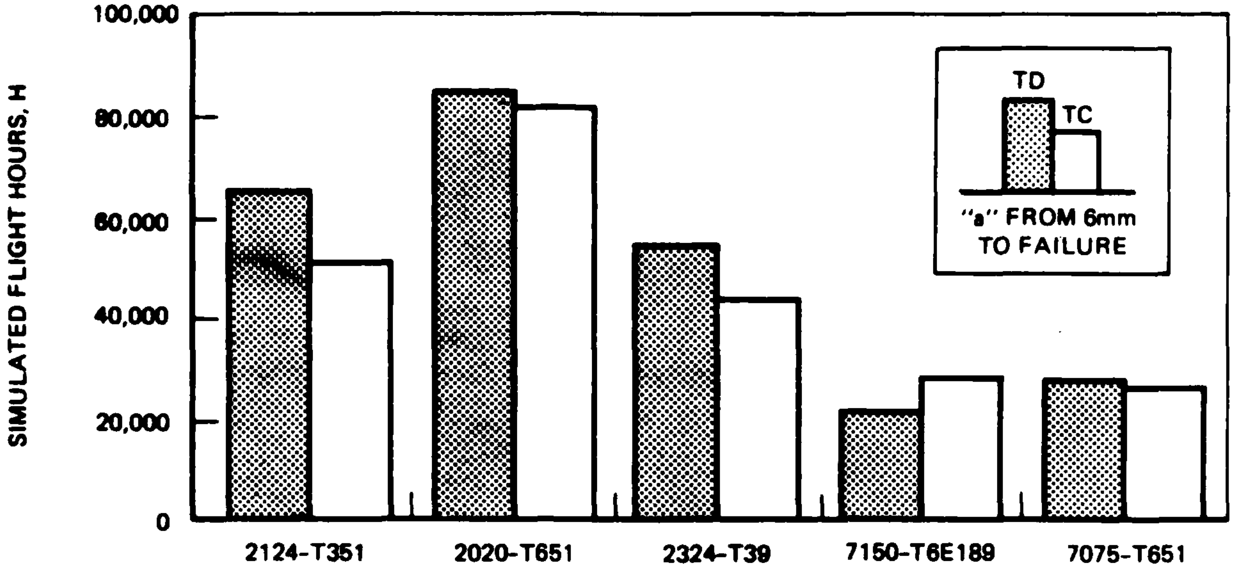

a. SPECTRUM LIFE AT 103 MPa. THE MATERIALS ARE LISTED IN DESCENDING ORDER FOR LIFE AT 145 MPa

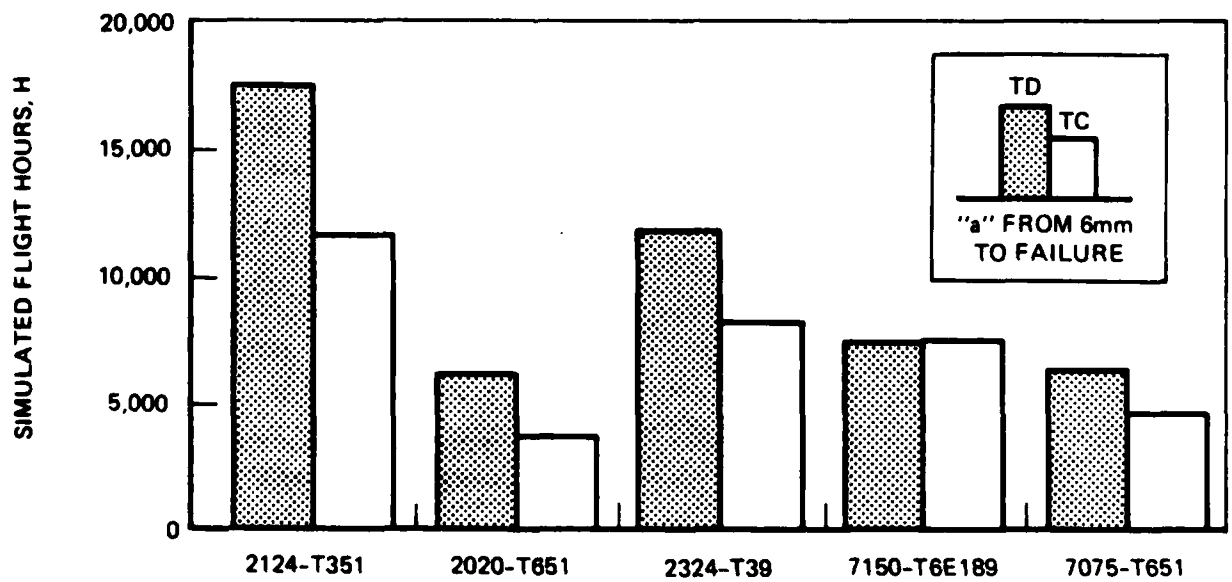

b. SPECTRUM LIFE AT 169 MPa. THE MATERIALS ARE LISTED IN DESCENDING ORDER FOR LIFE AT 145 MPa

FIGURE 12. SPECTRUM FATIGUE LIVES AT 103 AND 169 MPa

0.75 in.). The shorter position represents the very lowest K_{hmax} value in the spectrum test, while the other position is the longest crack length (highest K_{hmax}) consistently attained for all alloys, regardless of toughness.

For 2124-T351, the fatigue fracture mechanism for both the TD and TC spectrums at all crack lengths consists predominantly of ductile "striation" formation, though it is not clear that these striations correspond to individual load excursions in the spectrums (Figures 13 through 16). Very little evidence of void coalescence at constituent particles is seen for the TD spectrum, even at 19 mm, as shown in Figures 13 and 14. Limited void growth is evident for the TC spectrum at the longer crack length, Figure 16, but the fracture mechanism remains predominantly ductile striation formation. There is some evidence of abrasion on the TC fractures (Figure 15 especially), as suggested by the smooth areas where the striations have been rubbed away. Such abrasion was observed in Phase I on TC fractures, and is consistent with the extensive compressive loading in this spectrum.

Striation formation is not as evident for 7150 (Figures 17 through 20). In this high strength, lower ductility alloy it is more difficult to achieve the high degree of crack tip plasticity and blunting which is necessary to form well-defined striations. Rather, the general fracture topography is banded in the direction of crack growth, reflecting the "pancaked" grain structure of this alloy (Figures 17 and 19, especially). Fracture of constituent particles occurs at higher K_{hmax} levels (Figure 18), along with some striated growth which is better seen in the TC spectrum, Figure 20. The presence of striations at high K_{hmax} levels shows that extensive crack-tip plasticity can be developed, but only at the higher strains which occur at these stress intensity levels. As was the case with 2124, some fracture surface abrasion is evident on the TC specimen of 7150, Figure 19, along with some debris believed to be the result of fretting between the mating fracture surfaces.

Figure 18 shows an abrupt transition from stable fatigue crack growth (characterized by indistinct striation formation) to unstable tearing (denoted by void coalescence); this does not correspond, however, to the onset of rapid fracture at the end of the fatigue test. Rather, this tear is one of a series of "pop-in" fractures which occur as the crack approaches a critical flaw size. Figure 21 shows a series of bands for both 2124 and 7150 at crack lengths approaching final fracture; the darker bands are stable growth,

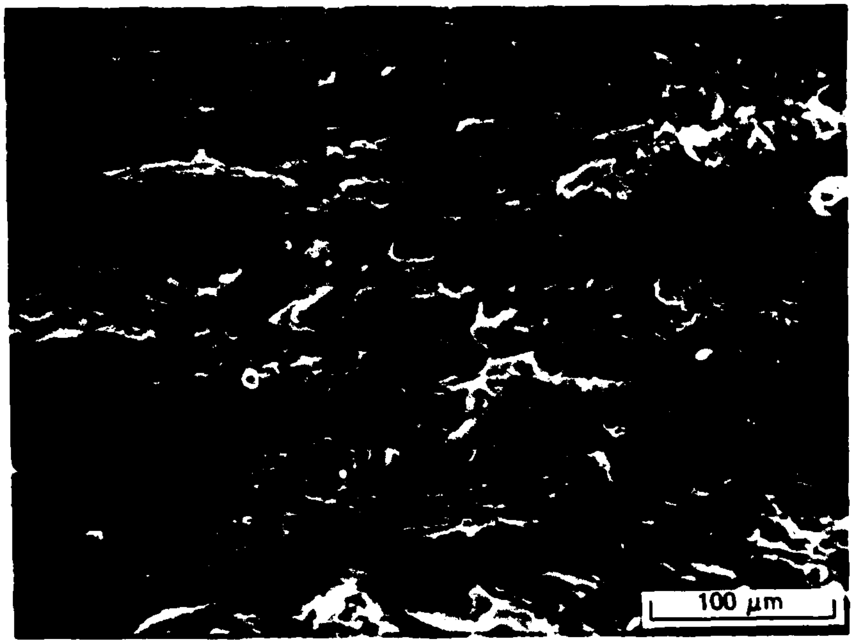

a. 250x 85-02224-1

CRACK GROWTH DIRECTION

b. 1500x 85-02224-2

FIGURE 13. FRACTURE SURFACE OF 2124-T351 TESTED USING TD SPECTRUM AT a = 6.4 mm (0.25 IN.)

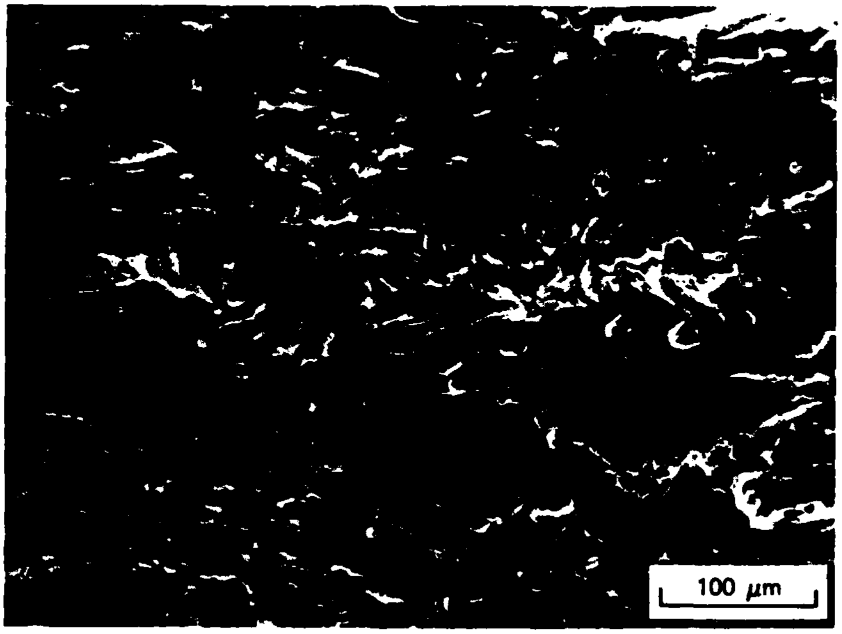

a. 250x 85-02218-1

CRACK GROWTH DIRECTION

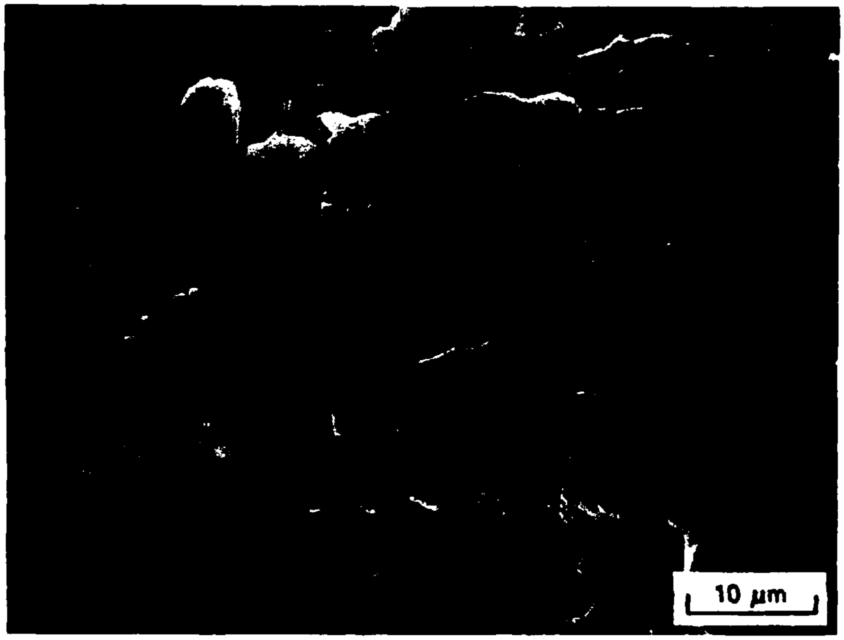

b. 85-02218-2

1500x

FIGURE 14. FRACTURE SURFACE OF 2124-T351 TESTED USING TD SPECTRUM AT a = 19.1 mm (0.75 IN.)

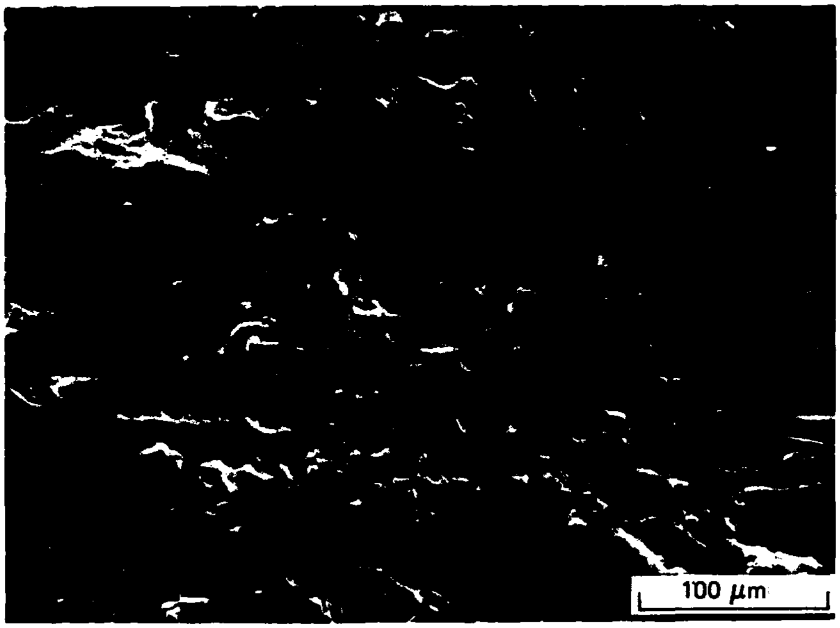

a. 250x 85-02220-1

CRACK GROWTH DIRECTION

b. 1500x 85-02220-2

FIGURE 15. FRACTURE SURFACE OF 2124-T351 TESTED USING TC SPECTRUM AT a = 6.4 mm (0.25 IN.)

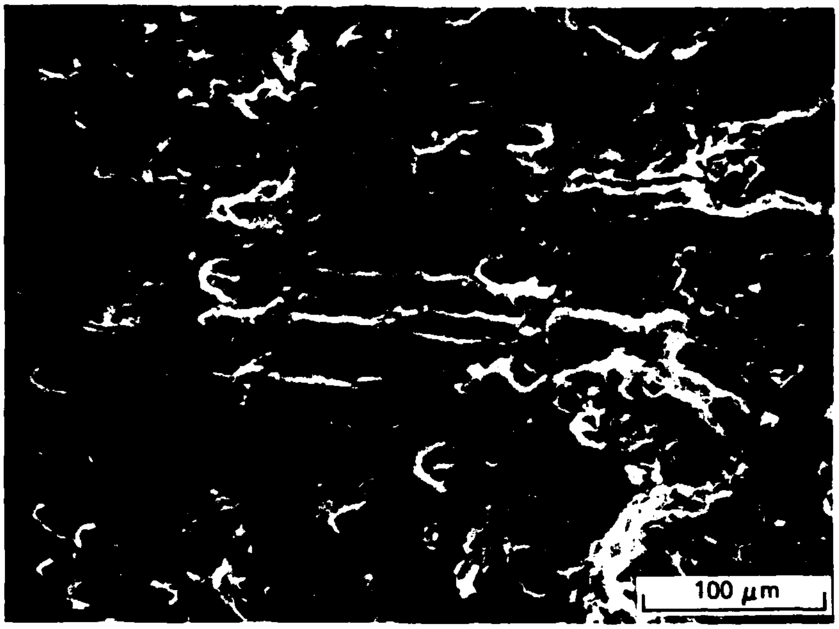

a. 250x 85-02217-1

CRACK GROWTH DIRECTION

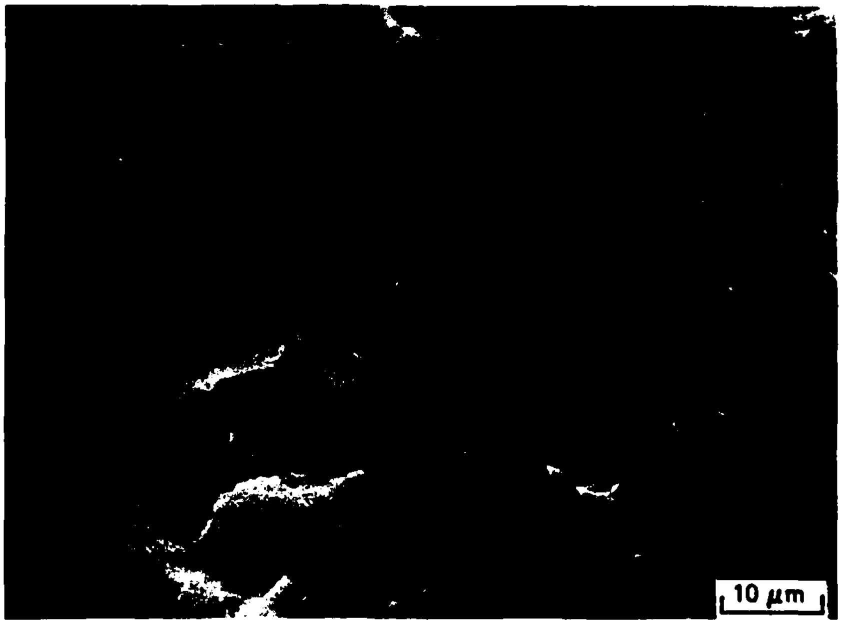

b. 1500x 85-02217-2

FIGURE 16. FRACTURE SURFACE OF 2124-T351 TESTED USING TC SPECTRUM AT a = 19.1 mm (0.75 IN.)

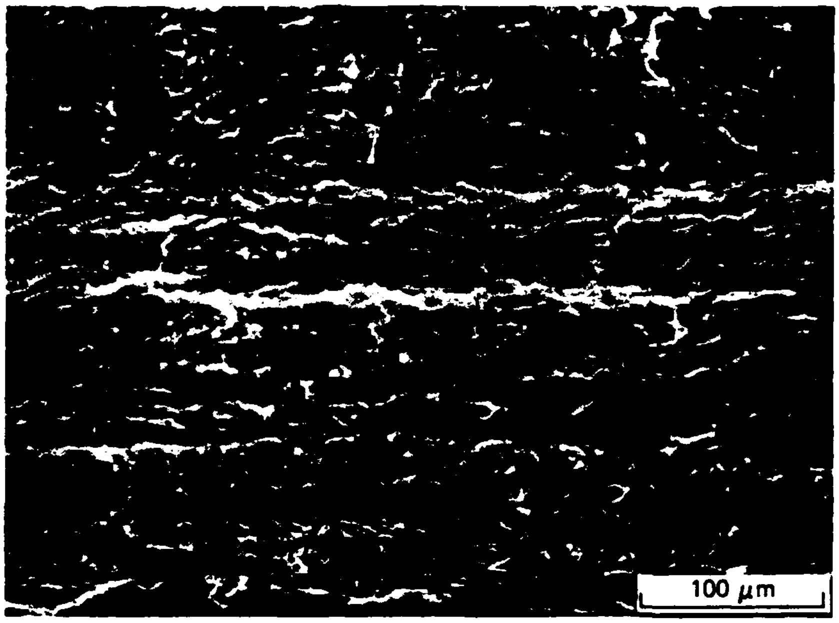

a. 250x 85-02222-1

CRACK GROWTH DIRECTION

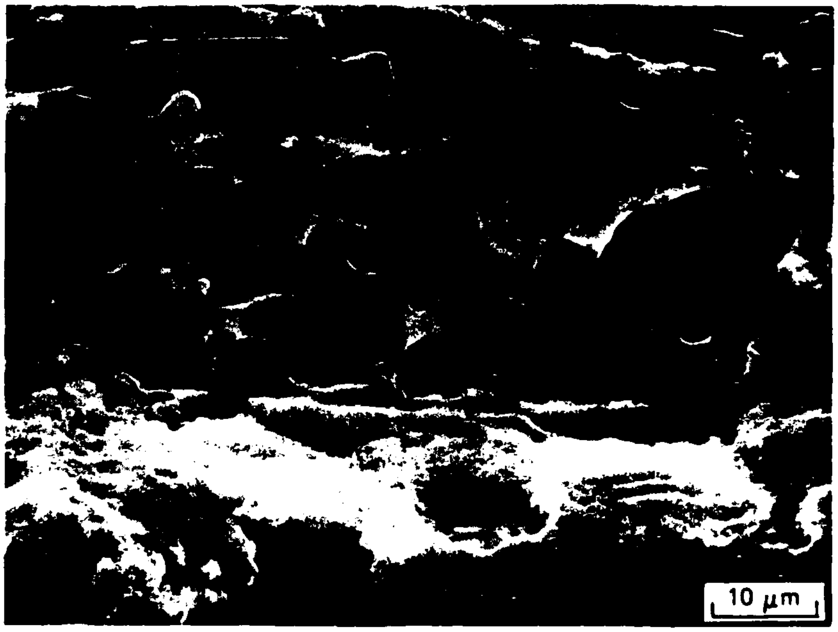

b. 1500x 85-02222-2

FIGURE 17. FRACTURE SURFACE OF 7150-T6E189 TESTED USING TD SPECTRUM AT a = 6.4 mm (0.25 IN.)

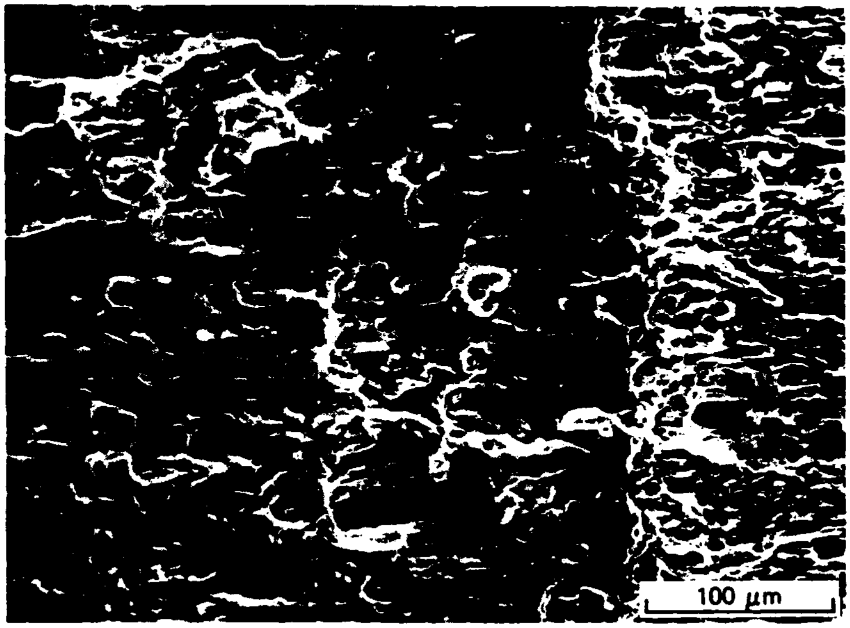

85-02225-1

a. 250x

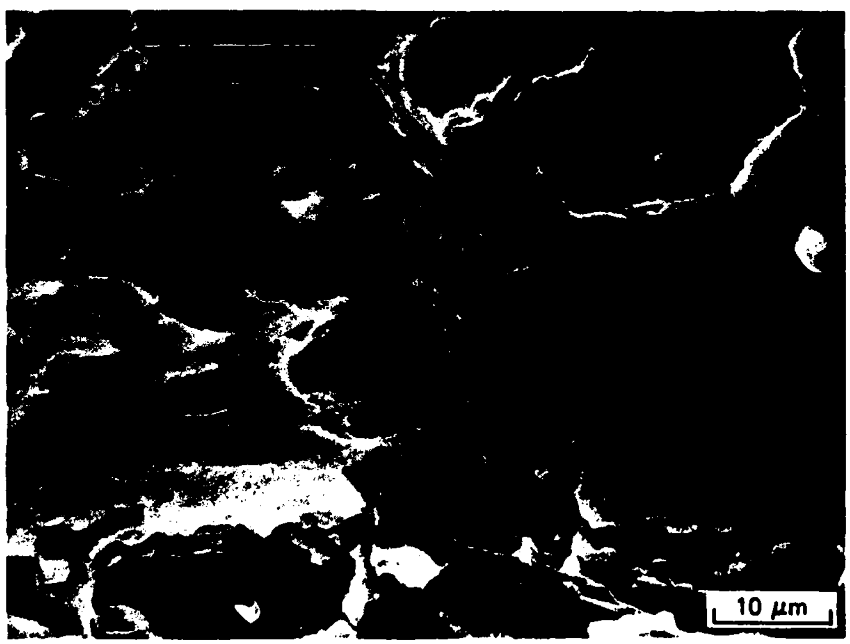

85-02225-2

b. 1500x

FIGURE 18. FRACTURE SURFACE OF 7150-T6E189 TESTED USING TD SPECTRUM AT a = 19.1 mm (0.75 in.) AREA IN b FROM STABLE FATIGUE REGION IN a

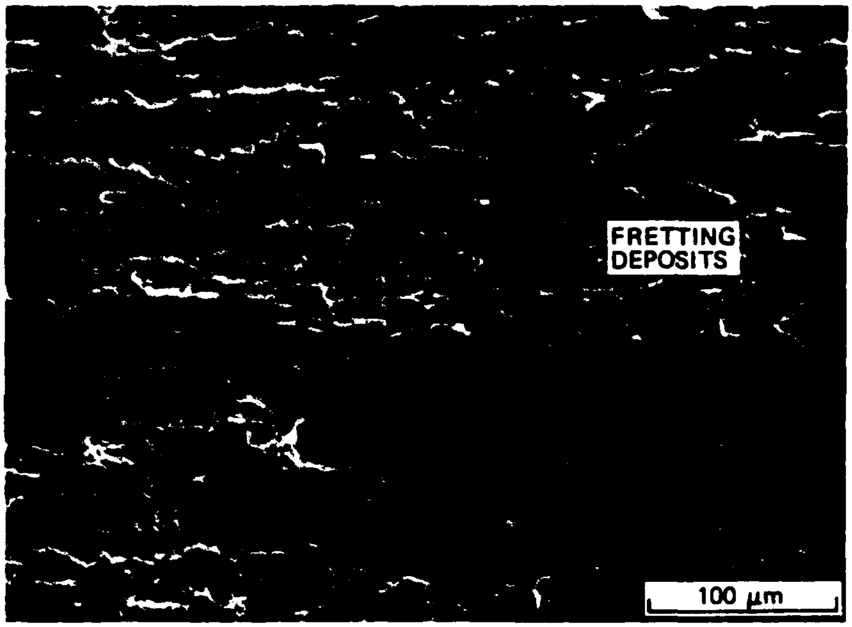

a. 250x 85-02234-1

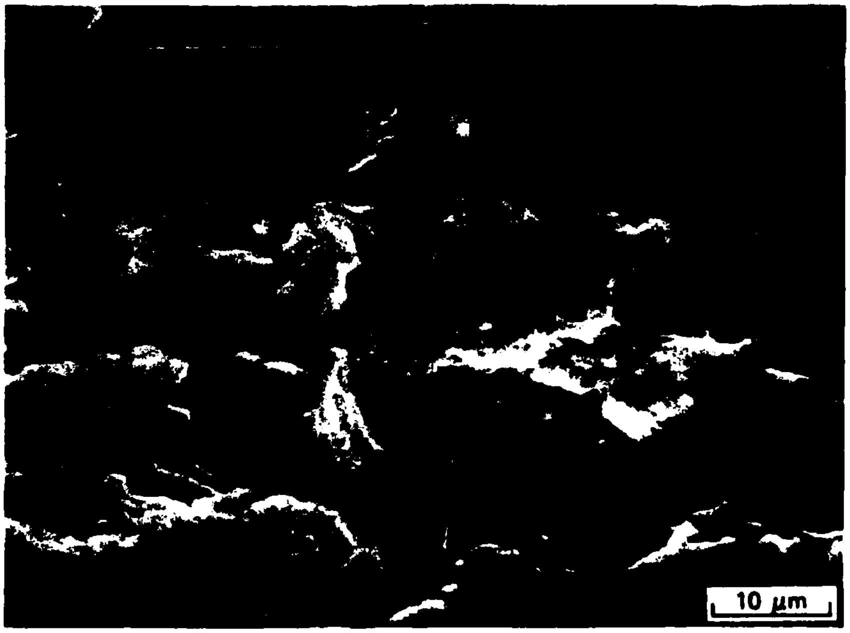

b. 1500x 85-02234-2

FIGURE 19. FRACTURE SURFACE OF 7150-T6E189 TESTED USING TC SPECTRUM AT a = 6.4 mm (0.25 IN.)

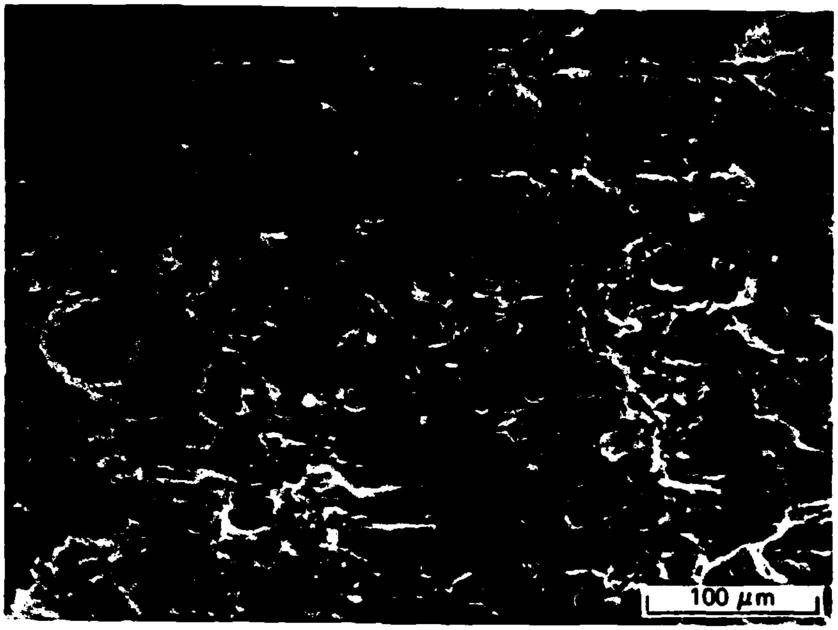

a. 250x 85-02221-1

CRACK GROWTH DIRECTION

b. 1500x 85-02221-2

FIGURE 20. FRACTURE SURFACE OF 7150-T6E189 TESTED USING TC SPECTRUM AT a = 19.1 mm (0.75 IN.)

FATIGUE | FRACTURE

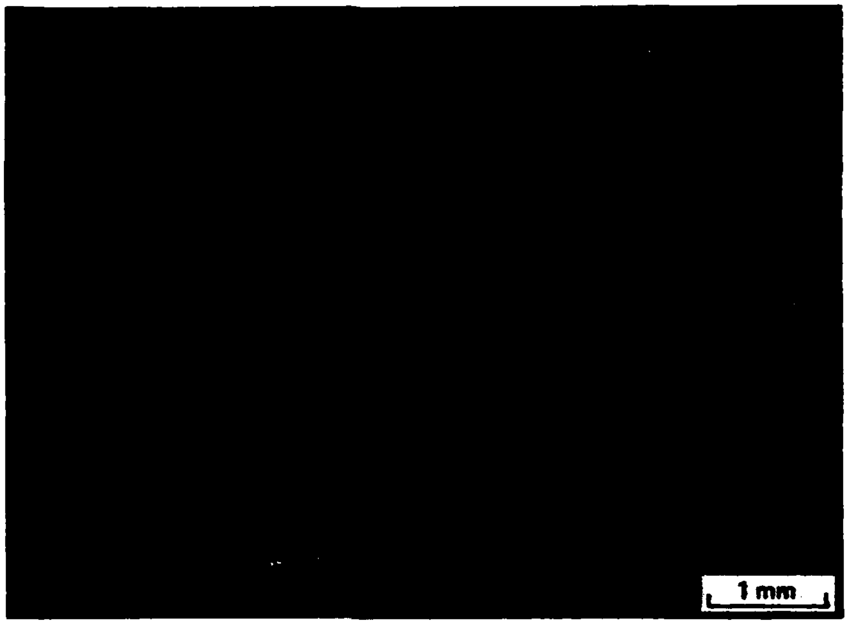

85-02223-1

a. 2124-T351 15x

NEAR FINAL FRACTURE

85-02223-2

b. 7150-T6E189 15x

FIGURE 21. BANDED FRACTURE SURFACES FOR 2124 AND 7150 PRIOR TO FINAL FRACTURE, INDICATING LOCAL TEARING DURING HIGH-SPECTRUM LOAD EXCURSIONS, BOTH TESTED USING TD SPECTRUM

while the lighter regions indicate local tearing instability. Presumably, these local tears correspond with the highest load excursions in the spectrum.

3.7 MODIFIED SPECTRUMS

One of the goals of this overall program was to develop a simplified spectrum that would reduce the testing required to evaluate materials for their resistance to spectrum fatigue crack growth. Several evaluations in this program were performed wholly or in part to satisfy that goal – the racetrack spectrums, which eliminated the smaller amplitude cycles, and the TCZ spectrum, which determined the importance of compression cycles. Eight alloys were evaluated using these three modified spectrums. Seven of the alloys were evaluated in Phase II and the eighth, 2020-T651, was evaluated in this phase. The results are presented in Tables 9 and 10 and Figure 22. Another effort was analytic. This analysis was a modified Willenborg prediction method which used the yield strength and constant-amplitude FCG behavior to predict the spectrum life of the specimens used in this program and correlate those results to the actual lives. This has never before been possible for such a variety of aluminum alloys evaluated under the same conditions. Although high correlation was not expected, trends may have existed that would have suggested those aspects of the spectrum that were more significant to the life, those changes that were needed in the models or indicated indirectly, and those metallurgical features that were significant to spectrum fatigue crack growth. The techniques used and the results are presented in Appendix D. Overall, the correlation was good; however, the life predictions for one alloy, 7475-T651, were grossly underestimated. This alloy later had the longest life of all the 7000 series alloys evaluated but it was predicted to have the shortest life. This indicated that using this model to determine the significant metallurgical variables was not likely to succeed at this time.

TABLE 9. SPECTRUM FATIGUE RESULTS – MODIFIED SPECTRUMS

MAXIMUM PEAK STRESS, σ_{hmax} = 145 MPa (21 ksi)
CRACK GROWTH FROM 6mm (0.24 in.) TO FAILURE

SIMULATED FLIGHT HOURS, H			
SPECTRUM	TDR	TCR	TCZ
MATERIAL			
2020-T651	26,315	11,867	22,552 31,168
2024-T351	24,899	15,738	34,205 31,090
2024-T851	9,410	7,403	10,258 12,175
7050-T7451	16,787	13,501	19,096 19,346
7075-T651	12,600	9,526	13,039 14,975
7075-T7351	14,179	11,446	17,502 17,595
7475-T651	21,259	19,387	22,630 23,364
7475-T7351	13,785	13,011	19,140 20,268

TABLE 10. RANKING OF MATERIALS UNDER SPECTRUM LOADING – MODIFIED SPECTRUMS

a. σ_{hmax} = 145MPa FROM a = 6mm TO FAILURE

TDR SPECTRUM		
MATERIAL	SIMULATED FLIGHT HOURS[a]	RANKING UNDER TD SPECTRUM[b]
2020-T651	26,300	3
2024-T351	24,900	1
7475-T651	21,300	2
7050-T7451	16,800	5
7075-T7351	14,200	6
7475-T7351	13,800	4
7075-T651	12,600	7
2024-T851	9,400	8

b. TCR SPECTRUM		
MATERIAL	SIMULATED FLIGHT HOURS[a]	RANKING UNDER TC SPECTRUM[b]
7475-T651	19,400	2
2024-T351	15,700	1
7050-T7451	13,500	4
7475-T7351	13,000	3
2020-T651	11,900	5
7075-T7351	11,400	6
7075-T651	9,500	7
2024-T851	7,400	8

c. TCZ SPECTRUM		
MATERIAL	SIMULATED FLIGHT HOURS[c]	RANKING UNDER TC SPECTRUM[b]
2024-T351	32,600	1
2020-T651	26,500	5
7475-T651	23,000	2
7475-T7351	19,700	3
7050-T7451	19,200	4
7075-T7351	17,500	6
7075-T651	14,000	7
2024-T851	11,200	8

a ONE TEST RESULT ROUNDED TO NEAREST HUNDRED HOURS

b CONSIDERING THESE EIGHT ALLOYS

c AVERAGE OF TWO TEST RESULTS ROUNDED TO NEAREST HUNDRED HOURS

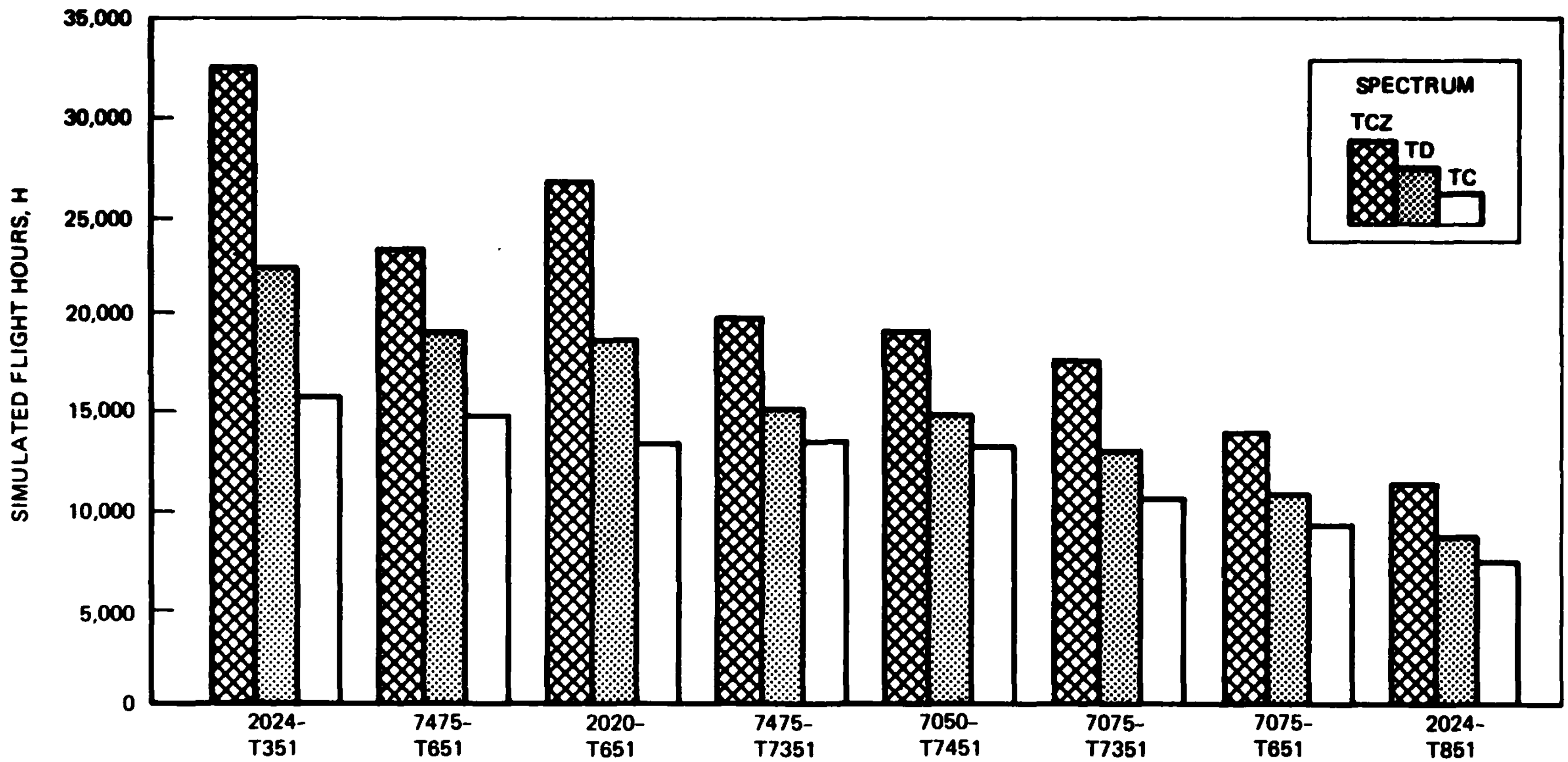

FIGURE 22. SPECTRUM FATIGUE LIVES FOR TCZ, TD, AND TC SPECTRUMS

4. SUMMARY AND CONCLUSIONS

An investigation to determine the important metallurgical factors that influence spectrum fatigue crack propagation (FCP) in selected high-strength aluminum alloys is being performed. This program was also designed to simplify complex load histories into generic simple spectrums and provide information for development and selection of fatigue resistant alloys. Most of the results on which this summary was based are discussed in the Phase II final report.[28] The results summarized herein represent a baseline characterization of a number of high-strength aluminum alloys, from which the selection, fabrication, and critical evaluation of alloys with systematically controlled microstructures followed – the results of which are described in a companion report.[29]

Twelve commercial 2XXX and 7XXX aluminum alloys were chosen for analysis so that the influence of both purity and temper on FCP could be evaluated. The alloys evaluated were 2020-T651, 2024-T351, 2024-T851, 2124-T351, 2124-T851, 2324-T39, 7050-T7451, 7075-T651, 7075-T7351, 7150-T6E189, 7475-T651, and 7475-T7351. All 12 alloys (seven in Phase I, three in Phase II, and two in Phase III) have been characterized with respect to chemical composition, microstructure, tensile properties, and fracture toughness. FCP tests were conducted on specimens of each alloy for both constant-amplitude loading (including the low ΔK region) and two F-18 load spectrums. The spectrum FCP testing was performed at a maximum peak stress of 145 MPa (21 ksi) as well as limited testing at 103 and 169 MPa (15 and 24.5 ksi) to obtain additional data at the low and high end of the crack growth range. Eight of the alloys were evaluated using three simplified spectrums. Pertinent fracture surface features were documented on the spectrum fatigue specimens.

The constant-load-amplitude FCP tests were performed on each material to provide a baseline characterization of steady-state FCP response. These data are necessary as inputs to life-prediction models. Fractographic analyses of these specimens are used to help explain the spectrum fatigue results.

The following observations can be made about the constant-load-amplitude FCP behavior of these alloys:

1. Rankings of constant-load-amplitude FCP resistance among the 12 materials are ΔK dependent

2. At near-threshold ΔK levels ($\leqslant 4$ MPa $\sqrt{m}$):

   a. Fatigue crack growth resistance varies more than that at higher ΔK levels

   b. 2124-T351 has greater crack growth resistance than the other 11 alloy-temper combinations

   c. FCP resistance of 7475-T651 exceeds that of the other five 7XXX alloys: 7075-T651, 7075-T7351, 7050-T7451, 7150-T6E189 and 7475-T7351

   d. These data confirm that:

      (1) Increased aging reduces near-threshold FCP resistance

      (2) Purity (Fe, Si content) has little or no effect on near-threshold crack growth rates

3. At intermediate ΔK levels (4 to 15 MPa $\sqrt{m}$):

   a. The 2XXX alloys, 2020-T651, 2124-T351, and 2324-T39, have lower FCG rates than the other alloys

   b. The peak aged 7XXX alloys, 7075-T651, 7150-T6E189, and 7475-T651, have faster FCG rates than the other alloys.

Spectrum FCP tests were conducted on each of the 12 alloys, using two complex F-18 load histories. The performance of each alloy in these spectrum tests and the relative rankings of the alloys represent valuable engineering information resulting in the selection of metallurgical variables that were systematically evaluated for their effects on fatigue crack growth as reported in Volume II of this report. Secondly, these results are baseline information for spectrum analyses and spectrum modifications. Several observations can be made based on the results for testing at the maximum peak stress of 145 MPa (21 ksi):

1. The ranking of the 12 alloys is the same for the two spectrums, except for 2020-T651 for which the ranking under the tension-compression (TC) spectrum is considerably lower than the tension-dominated (TD) spectrum.

2. For each material the TD spectrum consistently results in longer lives.

3. The differences in life between the two spectrums for the same alloy were relatively small - not more than 35 percent.

4. There were larger differences in lives among the 2XXX alloys than the 7XXX alloys; for example, a 100-percent difference for the TD spectrum between the two extremes for the 2XXX alloys - 2024-T851 and 2124-T351 - compared to a 55-percent difference between the extremes for the 7XXX alloys, 7475-T651, and 7075-T651.

5. A comparison of the spectrum lives and fatigue crack growth rates indicates that the overall spectrum life does not appear to be controlled by any particular regime of spectrum crack growth (or stress intensity).

In general, the spectrum performance rankings could not be correlated with yield strength or constant-amplitude FCP resistance at any ΔK level. However, spectrum performance could be correlated with fracture toughness; FCP life for both spectrums generally increased with increasing fracture toughness. Perhaps more significantly, the alloys that deform by planar slip generally had longer spectrum fatigue lives than those that deform more homogeneously.

Eight of the 12 alloys were spectrum fatigue tested using modifications of the baseline spectrums. Two different types of modifications were performed independently on the baseline spectrums. One modification had two goals:

1. Eliminate low-amplitude cycles to reduce testing time without changing the ranking (relative life) of the alloys

2. Determine the importance of low-amplitude cycles on the overall spectrum life.

The racetrack method was used to eliminate 43 percent of the low-amplitude cycles. Although the goal of preserving the same ranking as the baseline spectrums was not met, the differences in spectrum fatigue lives between the modified and baseline spectrums are small enough so that the selection of one alloy over another would not be significantly affected.

The second modification was made to determine the importance of compressive load cycles. To accomplish this, all compression load points were eliminated from the TC spectrum. There were significant increases in spectrum lives compared to the baseline spectrum; but surprisingly, the rankings of the eight alloys for this modified spectrum were the same as those for the two baseline spectrums except for 2020-T651 which performed relatively better under the TCZ spectrum.

A limited evaluation of a spectrum life prediction model indicated the inability of the model to predict the relative behavior these materials compared to their actual performance.

REFERENCES

1. Chanani, G.R., "Fundamental Investigation of Fatigue Crack Growth Retardation in Aluminum Alloys," AFML-TR-76-156, 1976.

2. Sanders, T.H., Sawtell, R.R., Staley, J.T., Bucci, R.J., and Thakker, A.B., "The Effect of Microstructure on Fatigue Crack Growth of 7XXX Aluminum Alloys Under Constant Amplitude and Spectrum Loading," NADC Contract No. N00019-76-C-0482, 1978.

3. Bucci, R.J., Thakker, A.B., Sanders, T.H., Sawtell, R.R., and Staley, J.T., "Ranking 7XXX Aluminum Alloy Fatigue Crack Growth Resistance Under Constant Amplitude and Spectrum Loading," ASTM STP 714, 1980.

4. Bucci, R.J., "Spectrum Loading – A Useful Tool to Screen Effects of Microstructure on Fatigue Crack Growth Resistance," ASTM STP 631, 1977.

5. Jonas, O., and Wei, R.P., "An Exploratory Study of Delay in Fatigue-Crack Growth," Int. J. of Fracture Mechanics, Vol 7, 1971, p. 116.

6. Schijve, J., "Effect of Load Sequences on Crack Propagation Under Random and Program Loading," Eng. Frac. Mech., Vol. 5, 1973, p. 269.

7. Stephens, R.I., Chen D.K., and Hom, B.W., "Fatigue Crack Growth With Negative Stress Ratio Following Single Overloads in 2024-T3 and 7075-T6 Aluminum Alloys," ASTM STP 595, 1976.

8. Alzos, W.X., Skat, A.C., Jr., and Hillberry, B.M., "Effect of Single Overload/Underload Cycles on Fatigue Crack Propagation," ASTM STP 595, 1976.

9. Chanani, G.R., "Effect of Thickness on Retardation Behavior of 7075 and 2024 Aluminum Alloys," ASTM STP 631, 1977.

10. Chanani, G.R., "Investigation of Effects of Saltwater on Retardation Behavior of Aluminum Alloys," ASTM STP 642, 1977.

11. Schijve, J., "Observations on the Prediction of Fatigue Crack Growth Propagation Under Variable-Amplitude Loading," ASTM STP 595, 1976.

12. Wanhill, R.J.H., "Maneuver Spectrum Fatigue Crack Propagation in Aluminum Alloy Sheet Materials," NLR-TR-78091-U, May 1980.

13. Dill, H.D., Saff, C.R., and Potter, J.M., "Effects of Fighter Attack Spectrum on Crack Growth," ASTM STP 714, 1980.

14. Abelkis, P.R., "Effect of Transport Aircraft Wing Loads Spectrum Variation on Crack Growth," ASTM STP 714, 1980.

15. Staley, J.T., "Microstructure and Toughness of High Strength Aluminum Alloys," ASTM STP 605, 1976.

16. Truckner, W.G., Staley, J.T., Bucci, R.J., and Thakker, A.B., "Effects of Microstructure on Fatigue Crack Growth of High Strength Aluminum Alloys," AFML-TR-76-169, 1976.

17. Staley, J.T., Truckner, W.G., Bucci, R.J., and Thakker, A.B., "Improving Fatigue Resistance of Aluminum Aircraft Alloys," Aluminum, 11, 1977, p. 53.

18. Sanders, T.H., Jr., and Staley, J.T., "Review of Fatigue and Fracture Research on High-Strength Aluminum Alloys," Fatigue and Microstructure, Metals Park: American Society for Metals, 1979.

19. Bretz, P.E., Vasudevan, A.K., Bucci, R.J., and Malcolm, R.C., "Effect of Microstructure on 7XXX Aluminum Alloy Fatigue Crack Growth Behavior Down to Near-Threshold Rates," Final Report, Naval Air Systems Command, Contract N00019-79-C-0258, 1981.

20. Willenborg, J., Engle, R.M., and Wood, H.A., "A Crack Growth Retardation Model Using an Effective Stress Concept," TM-71-1-FBR, WPAFB, Ohio, 1971.

21. Wheeler, O.E., "Crack Growth Under Spectrum Loading," J. of Basic Eng., Trans. ASME, March 1972, p. 181.

22. Elber, W., "The Significance of Fatigue Crack Closure," ASTM STP 1971, p. 486.

23. Dill, H.D., and Saff, C.R., "Effects of Fighter Attack Spectrum on Crack Growth," AFFDL-TR-76-112, March 1977.

24. Chanani, G.R., and Mays, B.J., "Observation of Crack-Closure Behavior After Single Overload Cycles in 7075-T6 SEN Specimens," Eng. Fract. Mech., Vol. 9, 1977, p. 65.

25. Chanani, G.R., "Determination of Plastic-Zone Sites at Fatigue Cracks by Optical Interference Technique," Int. J. of Fracture, Vol. 13, 1977, p. 394.

26. Jones, R.L., and Cagle, T.E., "The Mechanical Stress-Corrosion, Fracture Mechanics, and Fatigue Properties of 7050, 7475, and Ti-8Mo-8V-2Fe-3Al Plate and Sheet Alloys," Report FGT-5791, General Dynamics, 1976.

27. Chanani, G.R., Telesman, I., Bretz, P.E., and Scarich, G.V., "Methodology for Evaluation of Fatigue Crack-Growth Resistance of Aluminum Alloys Under Spectrum Loading," Technical Report (Phase I, Final Report), Naval Air Systems Command, Contract N00019-80-C-0427, April 1982.

28. Scarich, G.V., and Bretz, P.E., "Investigation of Fatigue Crack Growth Resistance of Aluminum Alloys Under Spectrum Loading," Technical Report (Phase II, Final Report). Naval Air Systems Command, Contract N00019-81-C-0550, April 1983.

29. Scarich, G.V., Bresnahan, K.M., and Bretz, P.E., "Fatigue Crack-Growth Resistance of Aluminum Alloys Under Spectrum Loading, Volume II – Aluminum Lithium Alloys," Technical Report, Naval Air System Command, Contract N00019-82-C-0425, December 1985.

30. Chanani, G.R., Scarich, G.V., Bretz, P.E., and Sheinker, A.A., "Spectrum Fatigue Crack Growth Behavior of Aluminum Alloys," Proceedings of the Sixth International Conference on Fracture (ICF6), New Delhi, India, Vol. 3, 1984, p. 1609.

31. Scarich, G.V., Gambone, M.J., Chanani, G.R., and Bretz, P.E., "Correlation of Fatigue Behavior With Microstructure of 2XXX and 7XXX Aluminum Alloys," Proceedings of the Sixth International Conference on Fracture (ICF6), New Delhi, India, Vol. 3, 1984, p. 2015.

APPENDIX A

CONSTANT AMPLITUDE FATIGUE CRACK-GROWTH RATE, da/dN VERSUS ΔK

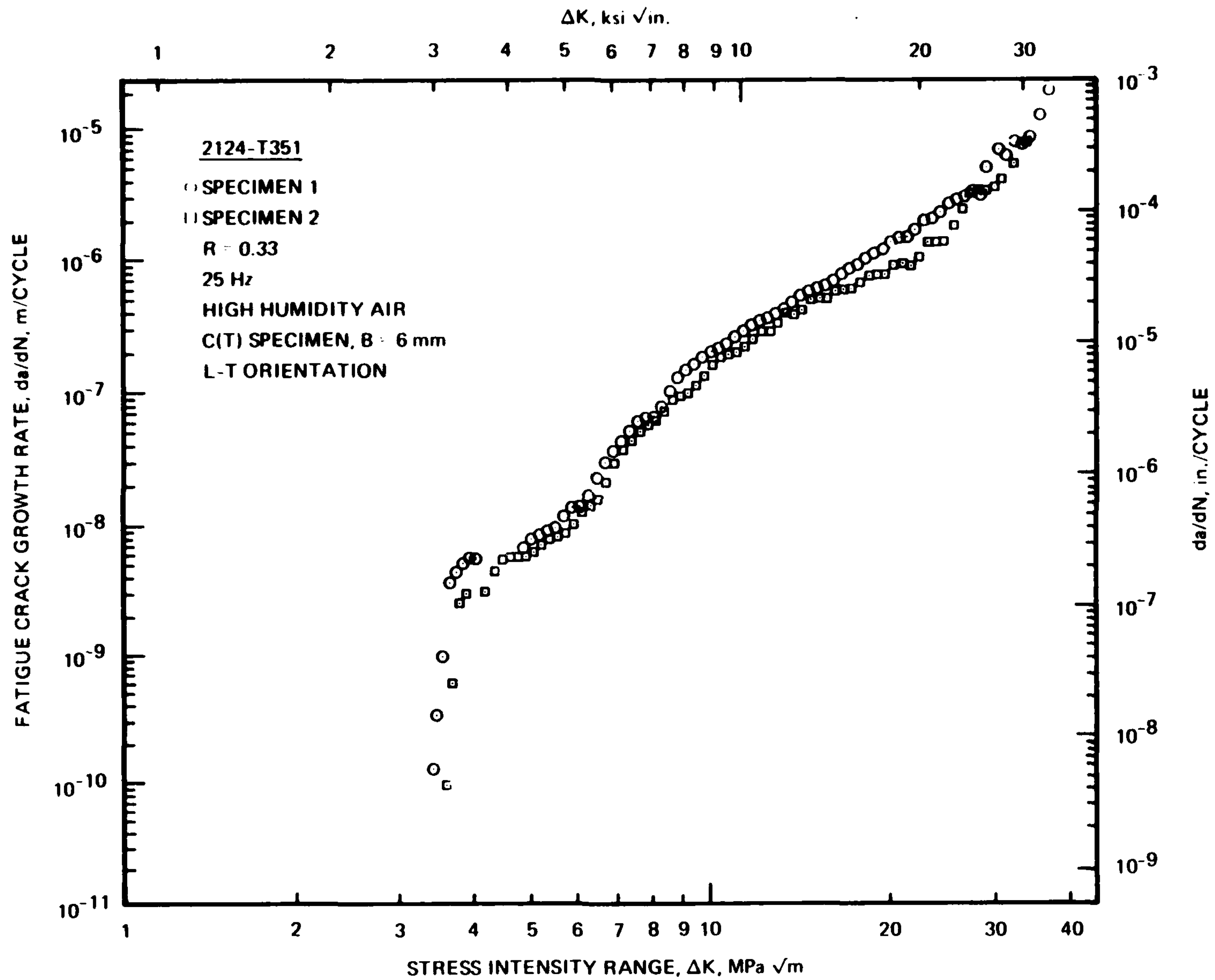

FIGURE A-1. CONSTANT-LOAD-AMPLITUDE FATIGUE CRACK GROWTH RATE DATA FOR 2124-T351

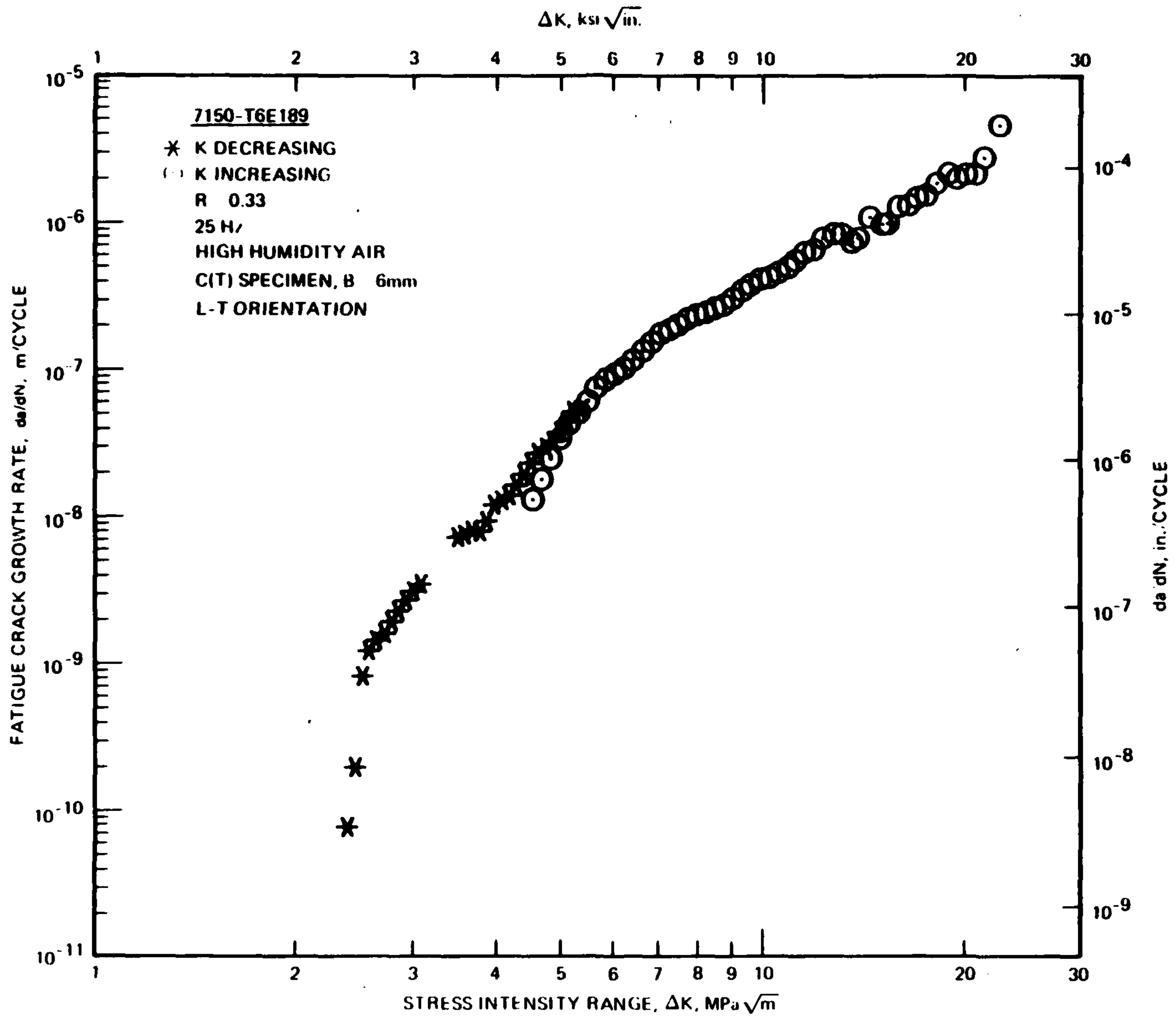

FIGURE A-2. CONSTANT-LOAD-AMPLITUDE FATIGUE CRACK GROWTH RATE DATA FOR 7150-T6E189

APPENDIX B

CRACK LENGTH VERSUS SIMULATED FLIGHT HOURS FOR BASELINE SPECTRUMS, a VERSUS H

1. The scale for the ordinate (a) is the same for each graph; the scale for the abscissa (H) varies, and to make comparisons easier, the abscissa was adjusted so that a crack length of 6 mm corresponded to zero simulated flight hours.

2. Two specimens each were tested at 145 MPa, and one each at 103 and 169 MPa.

3. Data are in numerical order by alloy designation with TD spectrum first, then TC spectrum.

4. The tension-dominated (TD) spectrum representing the lower wing root load history of the F-18 is coded C2 at Northrop and the tension-compression (TC) spectrum representing the horizontal hinge tail moment load history is coded E3.

5. Crack length was measured at the end of one or more passes (300 simulated flight hours per pass) of the spectrum, which at the beginning of the 103 and 145 MPa tests resulted in the crack growth increment being less than 0.25 mm which is required by ASTM E647. (Note that ASTM E647 is a method for constant amplitude fatigue crack-growth.) However, in calculating crack growth rates, the 0.25 mm increment requirement was observed. At the higher crack-growth rates, the one-per-pass crack measurement resulted in larger crack-growth increments than required by ASTM E647.

6. Graphs were plotted using a Northrop Support Services Laboratory computer program designated $DDNPT1 from data on files designated .DDN, created from crack length measurement versus pass raw data.

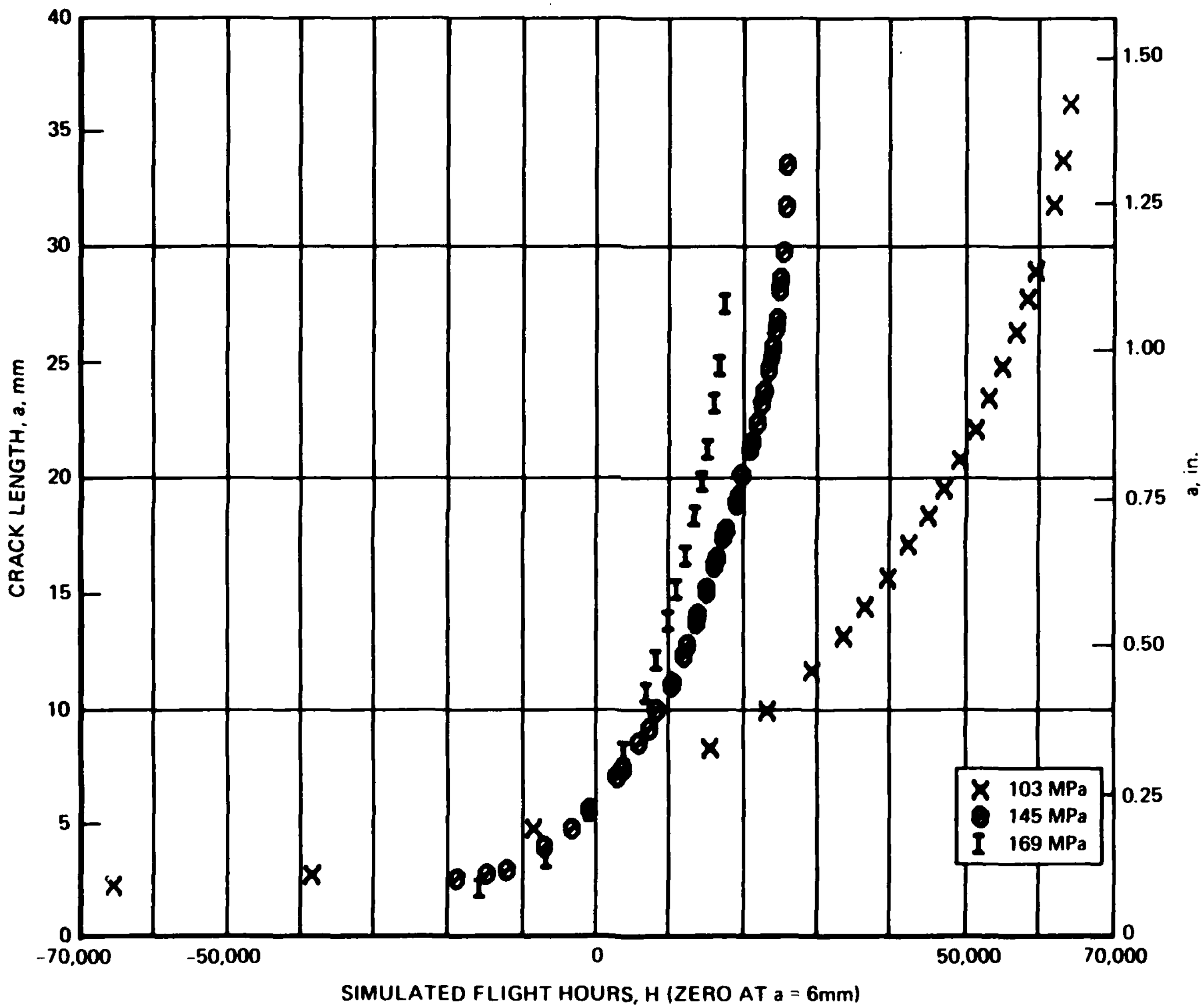

FIGURE B-1. 2124-T351,TD SPECTRUM

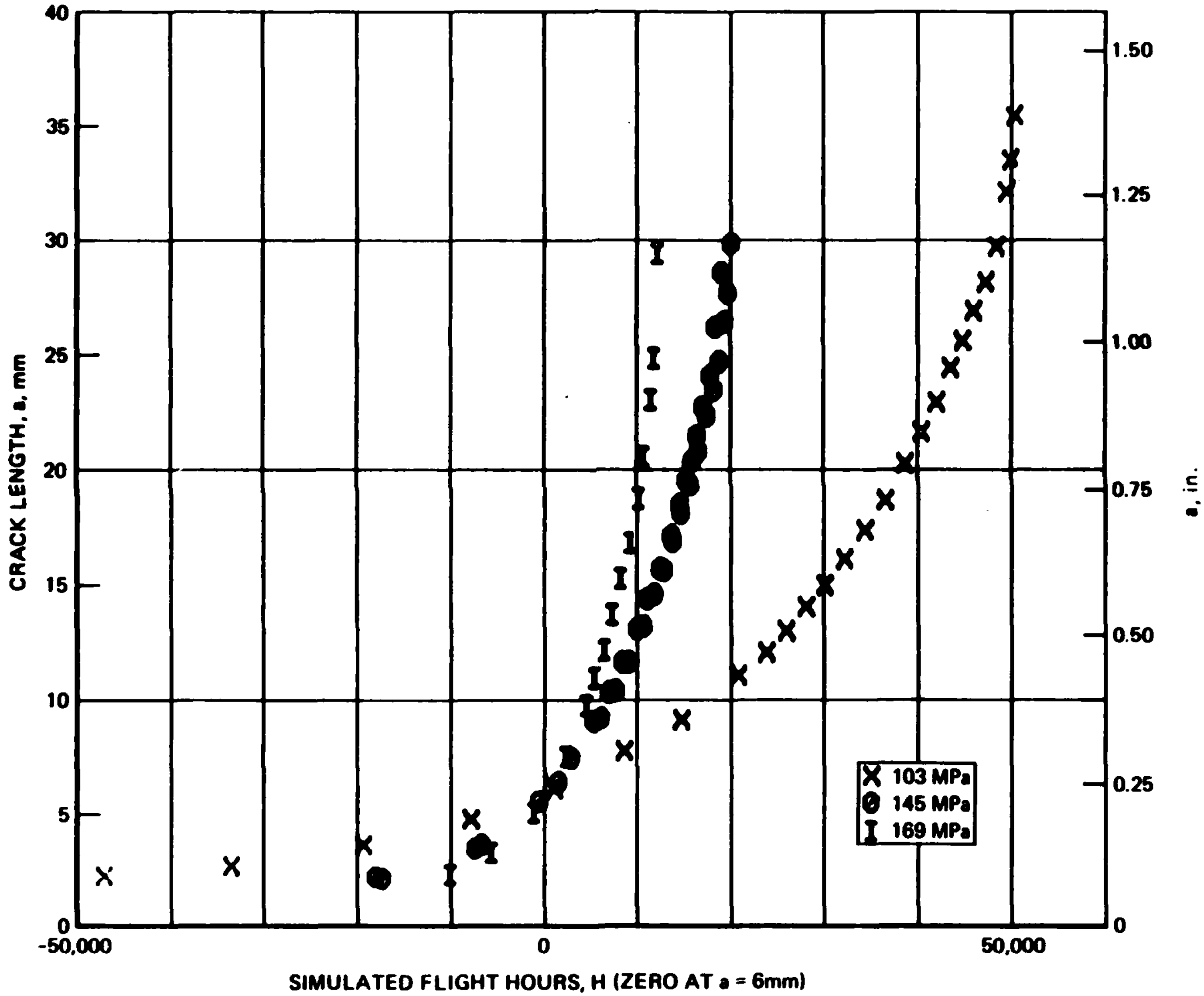

FIGURE B-2. 2124-T351,TC SPECTRUM

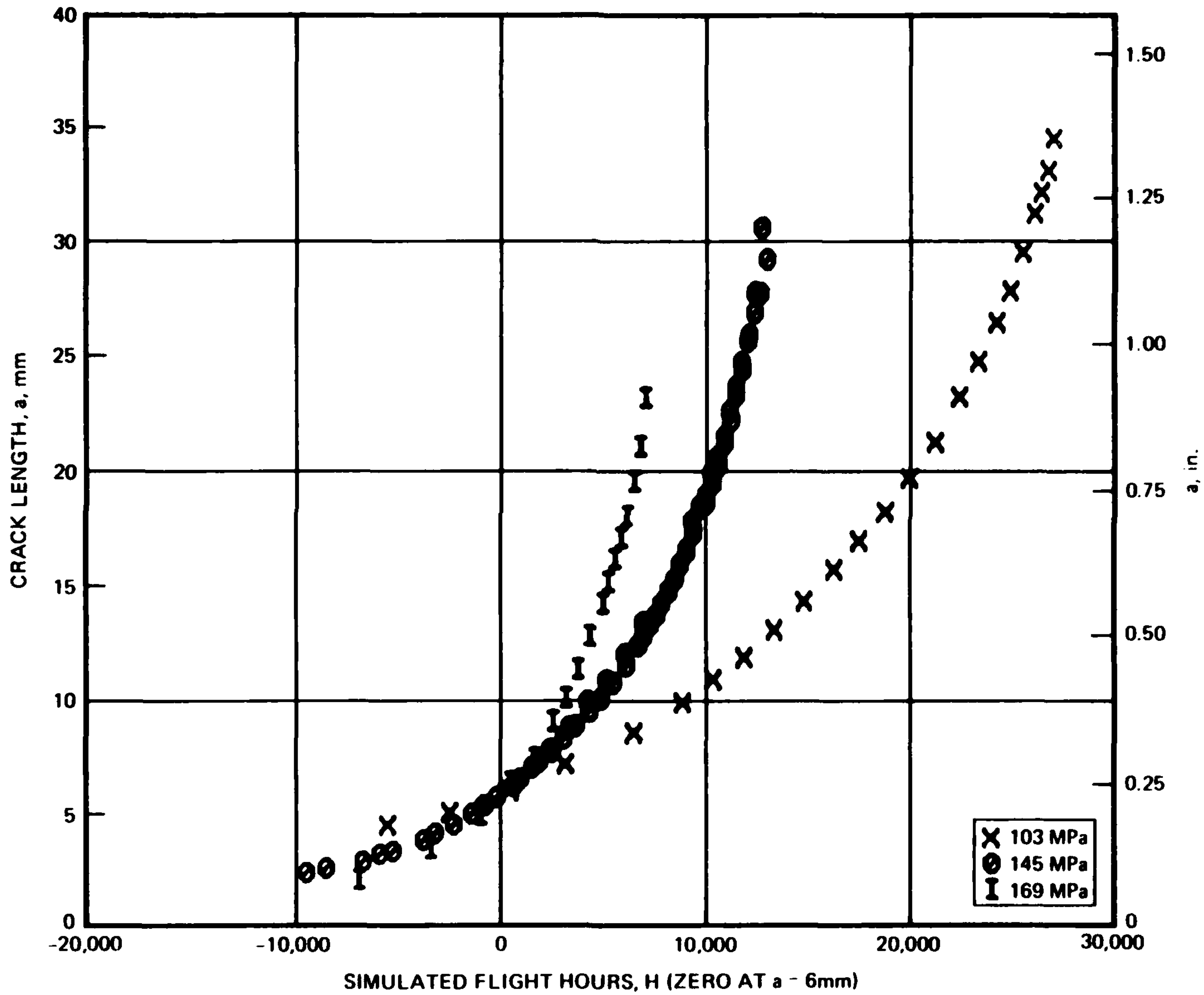

FIGURE B-3. 7150-T6E189, TD SPECTRUM

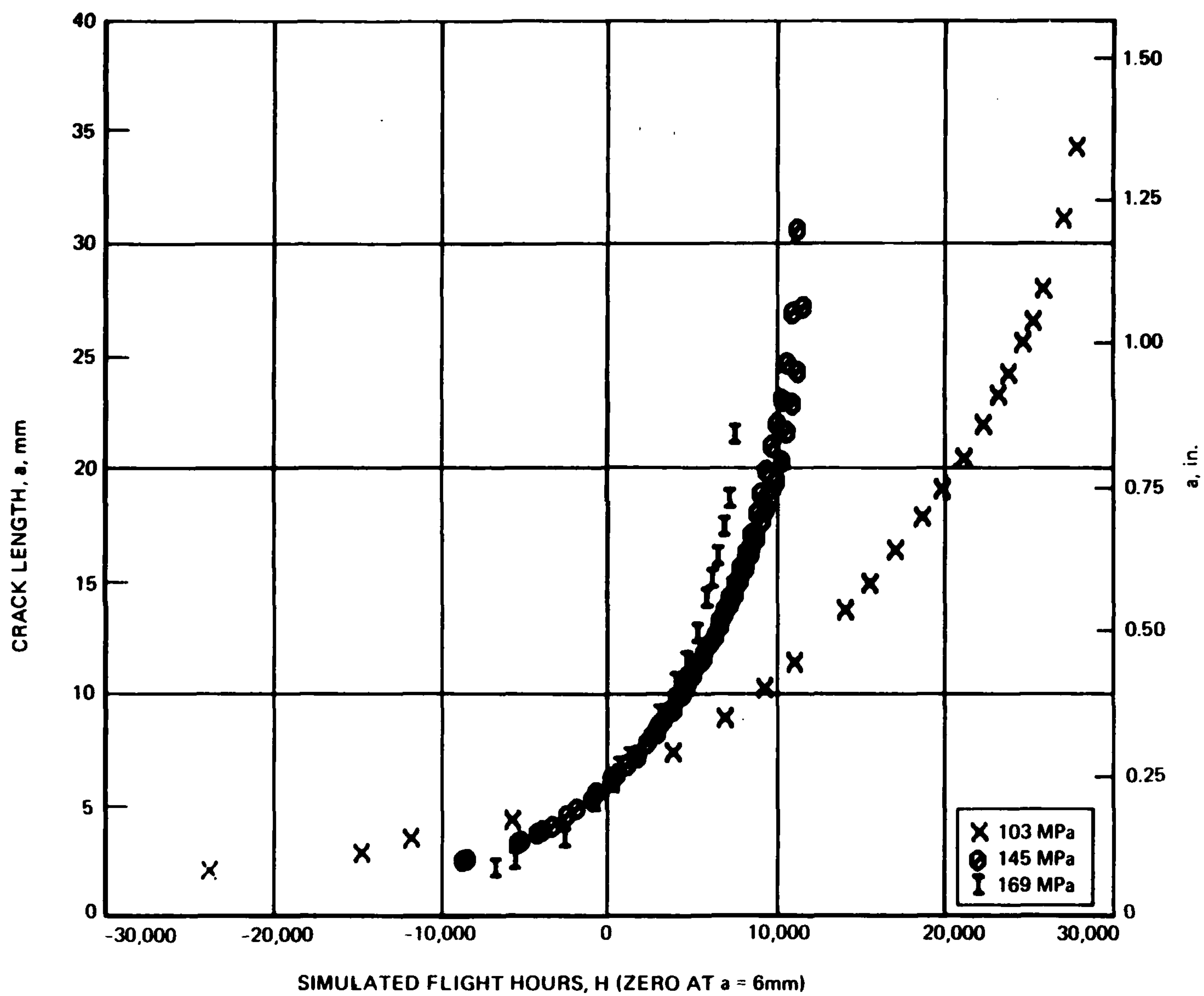

FIGURE B-4. 7150-T6E189, TC SPECTRUM

APPENDIX C

SPECTRUM CRACK GROWTH RATE VERSUS MAXIMUM PEAK STRESS INTENSITY da/dH VERSUS K_{hmax}

1. The scales for both axes are identical on each graph.

2. Crack growth rates are calculated by the two-point secant method per ASTM E647 based on the data in Appendix B, and applying the ASTM E647 requirement that the minimum crack growth interval, a, be greater than or equal to 0.25 mm. This is performed using Northrop Support Services Laboratory computer program designated $FITPTO from data on files designated .DDN, created from crack length measurement versus pass raw data. The data are plotted with a program designated $SPCPT1.

3. Almost all tests had a crack growth rate which initially decreased for a few data points after precracking; therefore, all data up to the first local minimum crack growth rate were not plotted.

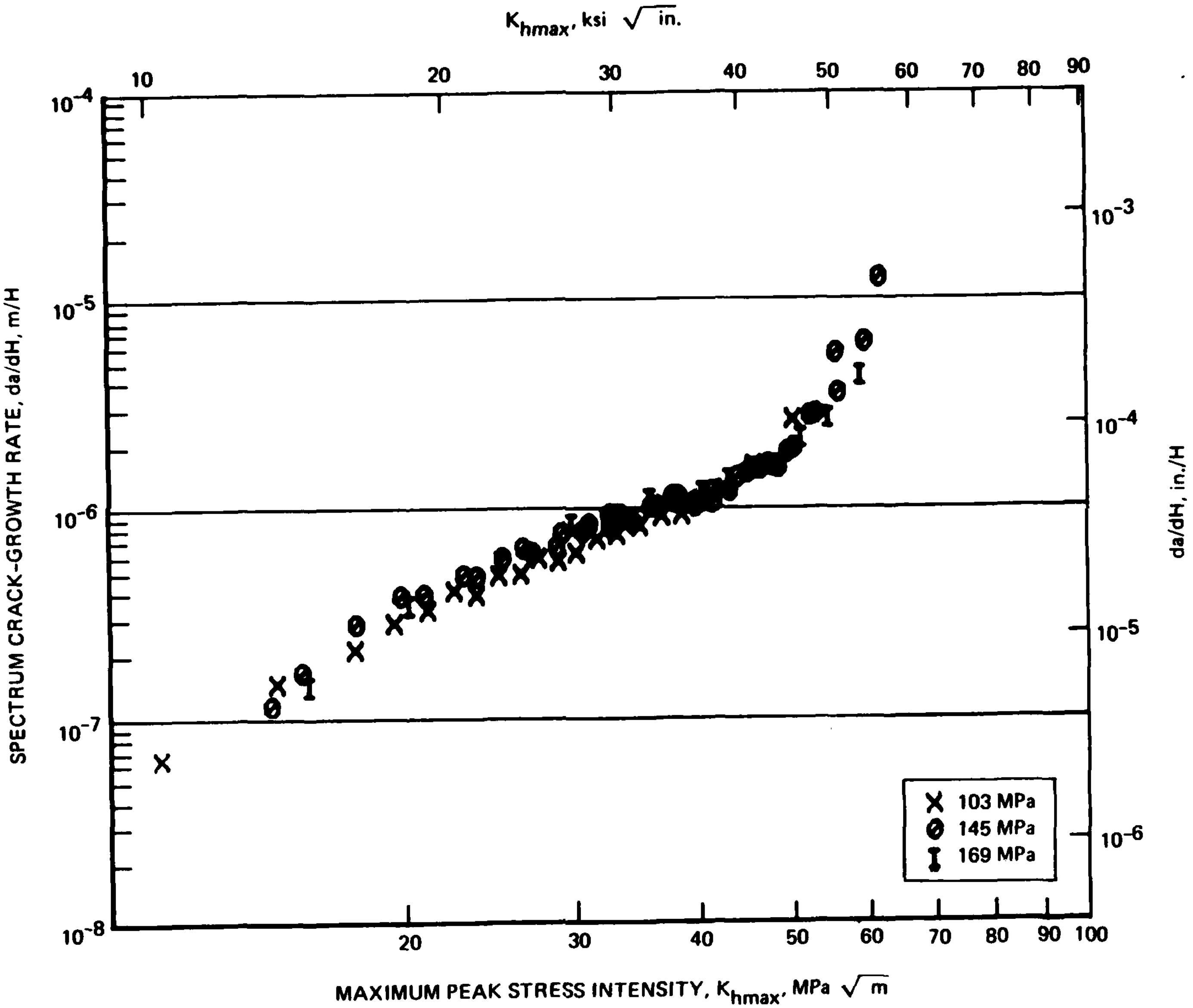

FIGURE C-1. 2124-T351, TD SPECTRUM

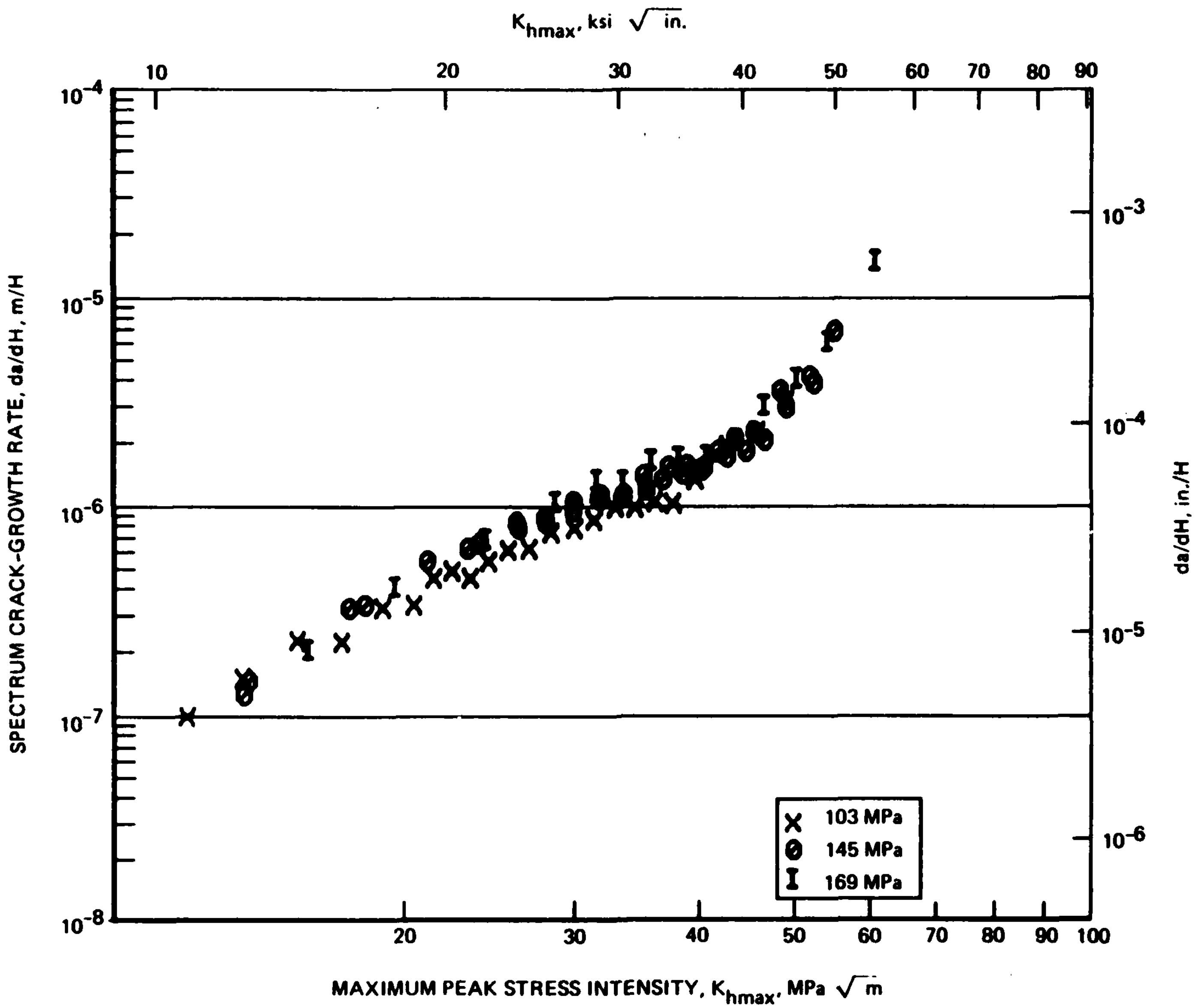

FIGURE C-2. 2124-T351, TC SPECTRUM

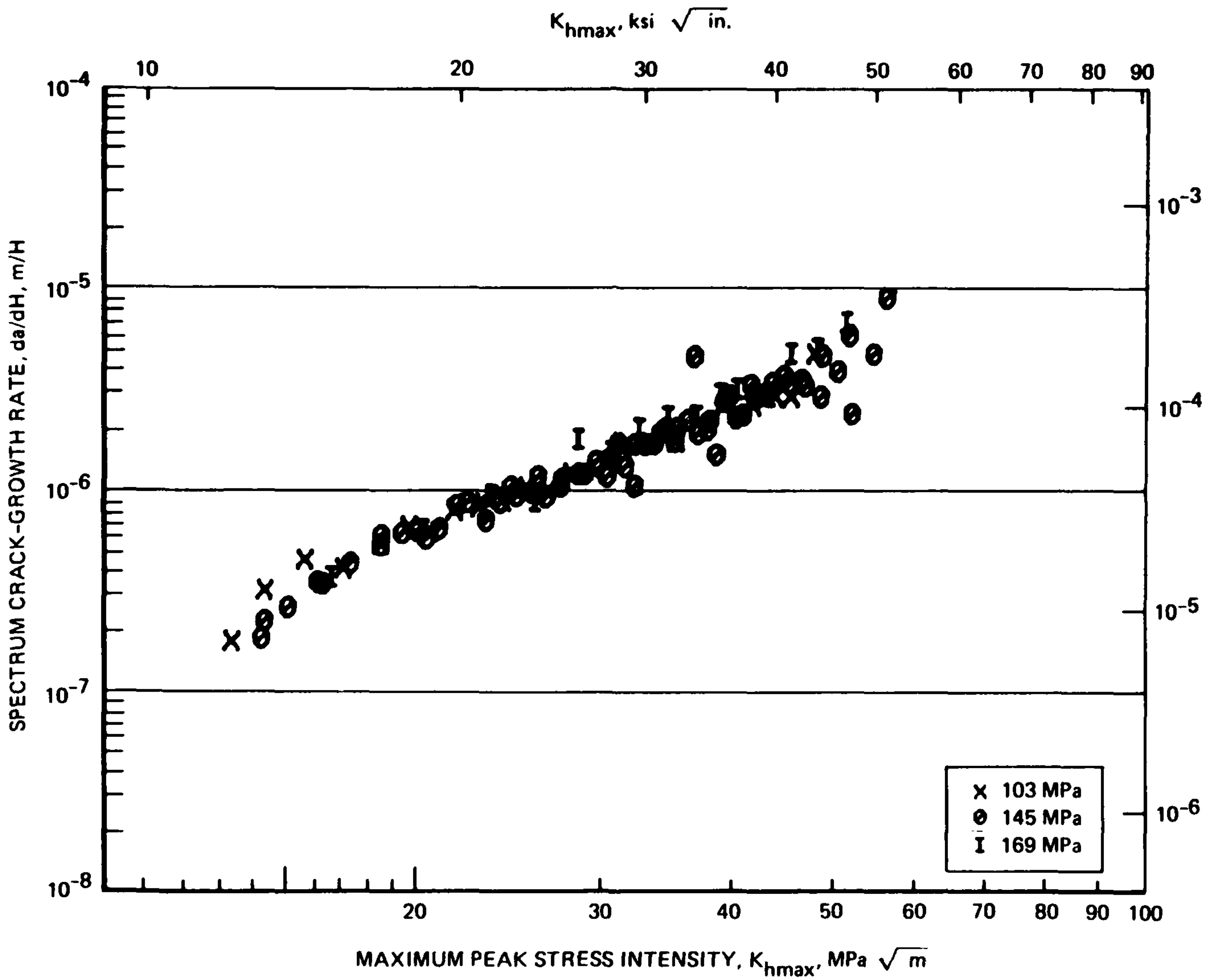

FIGURE C-3. 7150-T6E189, TD SPECTRUM

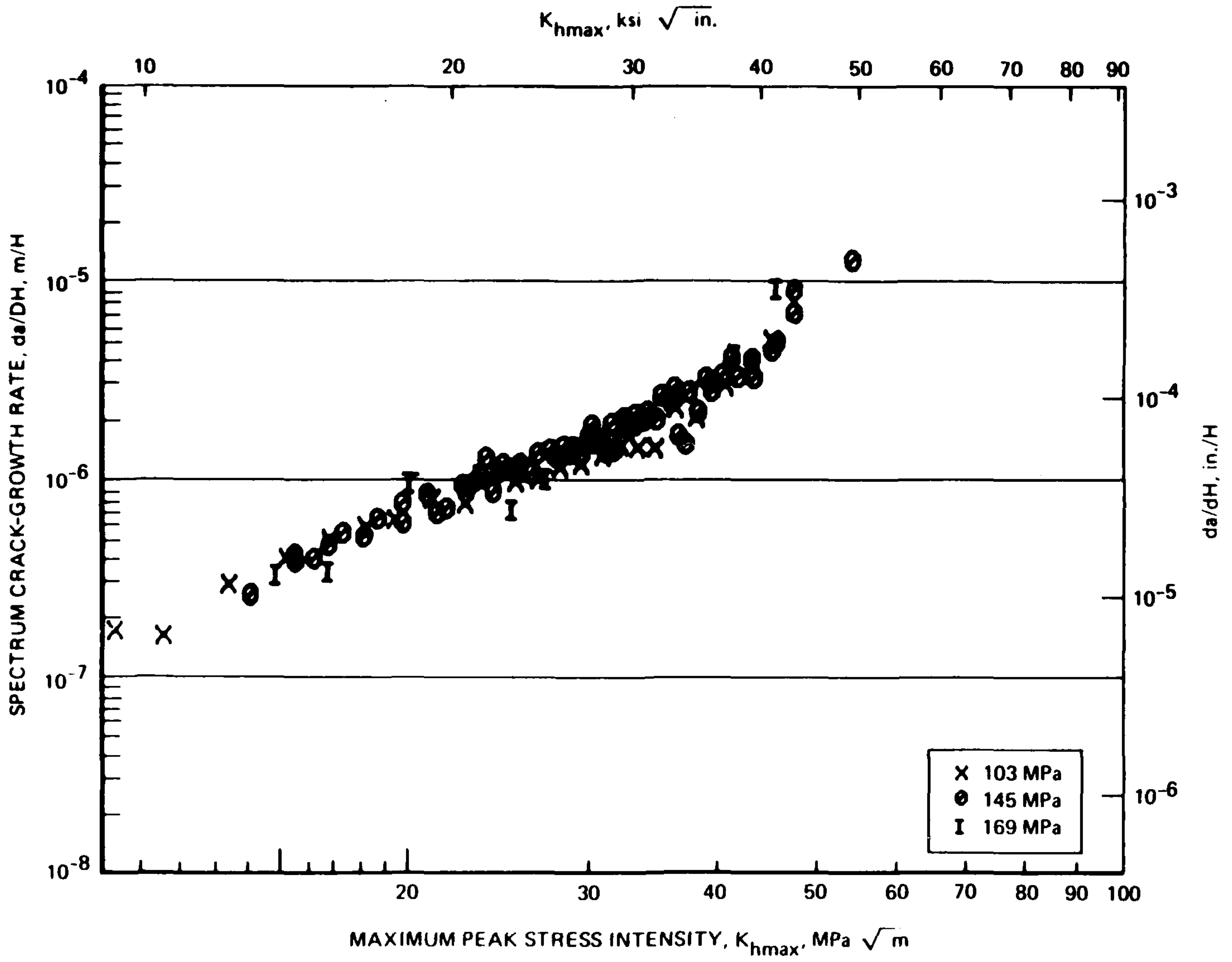

FIGURE C-4. 7150-T6E189, TC SPECTRUM

APPENDIX D

PREDICTION

Spectrum fatigue crack growth analyses were conducted on 10 alloys under two F-18 aircraft spectrums for a truncation of these two spectrums. These spectrums were a tension-dominated wing spectrum (TD), a tension-compression tail spectrum (TC), and the racetrack modification of these two spectrums (TDR and TCR).

The NORCRAK program was used to predict the spectrum crack growth lives. This program sums incremental crack growth on a cycle-by-cycle basis. It uses the Paris, Forman, or Walker equations, or tabulated da/dN versus ΔK data to provide a crack growth rate basis. Retardation due to load interaction can also be accommodated using any of the Wheeler, Willenborg, or Northrop models. A number of commonly used stress intensity solutions are built into the program for use in the crack growth equations, and in addition it is possible to input K versus beta factors in tabular form for problems in which a K solution is not available. Tabulated data with a modified Willenborg retardation scheme was used for the present analyses. The K solution for the specimen was determined by combining (beta) factors for a center through crack and a crack emanating from a hole. The sensitivity to R ratio was based on data for 2024-T351 and 7075-T7351 and those sensitivities used for the 2000 and 7000 series alloys respectively.

The predictions for 7075-T7351 were normalized so that total life matched the test data for the two baseline (untruncated) spectrums. This was accomplished through the use of a "Shut-Off Load Ratio." This parameter was assumed to be only spectrum dependent and was utilized for all other predictions.

Total life predictions were made and the predicted spectrum lives were divided by the actual specimen lives and both are presented in Table D-1. A reasonable correlation was obtained for most materials. The most glaring exception was 7475-T651 which exhibited actual life far longer than predicted.

Life predictions were plotted in the form of crack length versus flight hours for 2024-T351, 7475-T651, and 7075-T7351 for the TD and TC spectrums. The general characteristic of all these predictions was that crack growth rate was underpredicted at short crack lengths and overpredicted at longer crack lengths. This can be seen in the K_{hmax} versus crack growth rate shown in Figure D-1. Note that the predicted and actual lives for 7075-T7351 were adjusted to be identical.

This rate error effect could be due to either geometrical parameter errors at short crack lengths or to stress intensity effects of some other nature. Other apparent errors are the effect of yield strength on retardation (no substantial effect was observed) and the neglect of compressive loads on retardation leading to different normalization for the TC versus TD spectrums.

TABLE D-1. SPECTRUM LIFE PREDICTIONS

AVERAGE ROUNDED TO NEAREST HUNDRED HOURS.
MAXIMUM PEAK STRESS, σ_{hmax} = 145 MPa, "a" FROM 6mm TO FAILURE.

a. TENSION-DOMINATED SPECTRUMS

MATERIAL	TD SPECTRUM			TDR SPECTRUM		
	SIMULATED FLIGHT HOURS		PREDICTED / ACTUAL	SIMULATED FLIGHT HOURS		PREDICTED / ACTUAL
	ACTUAL	PREDICTED		ACTUAL	PREDICTED	
2020-T651	18,500	18 900	1.02	26,300	18 900	0.72
2024-T351	22,100	22,500	1.02	24,900	21,600	0.87
2024-T851	8 500	8,100	0.95	9 400	8 100	0.86
2124-T851	11 200	10 200	0.91	–	–	–
2324-T39	17 800	13,500	0 76	–	-	–
7050-T7451	14 900	10,800	0 72	16 800	11 100	0.66
7075-T651	10 800	6 300	0 58	12,600	6 900	0 55
7075-T7351	12 900	12,200	1 00	14 200	13,200	0 87
7475-T651	19 000	4 800	0 25	21 300	4 800	0 23
7475-T7351	15 000	11 100	0.74	13,800	11 100	0 80

b TENSION-COMPRESSION SPECTRUMS

MATERIAL	TC SPECTRUM			TCR SPECTRUM		
	SIMULATED FLIGHT HOURS		PREDICTED / ACTUAL	SIMULATED FLIGHT HOURS		PREDICTED / ACTUAL
	ACTUAL	PREDICTED		ACTUAL	PREDICTED	
2020-T651	13 100	15 900	1 21			
2024-T351	15 400	16 500	1 07	15 700	16 500	1 05
2024-T851	7 100	6 600	0 93	7 400	6 300	0 85
2124-T851	9 100	8 700	0 96			
2324-T39	14 400	11 400	0 79			
7050-T7451	13 200	9 600	0 73	13 500	9 600	[illegible]
7075-T651	8 900	6 000	0 67	9 500	6 000	0 63
7075-T7351	10 700	10 800	1 01	11 400	10 800	0 95
7475-T651	14 900	4 500	0 30	19 400	4 500	0 23
7475-T7351	12 400	[illegible]	0 69	13 000	[illegible]	0 72

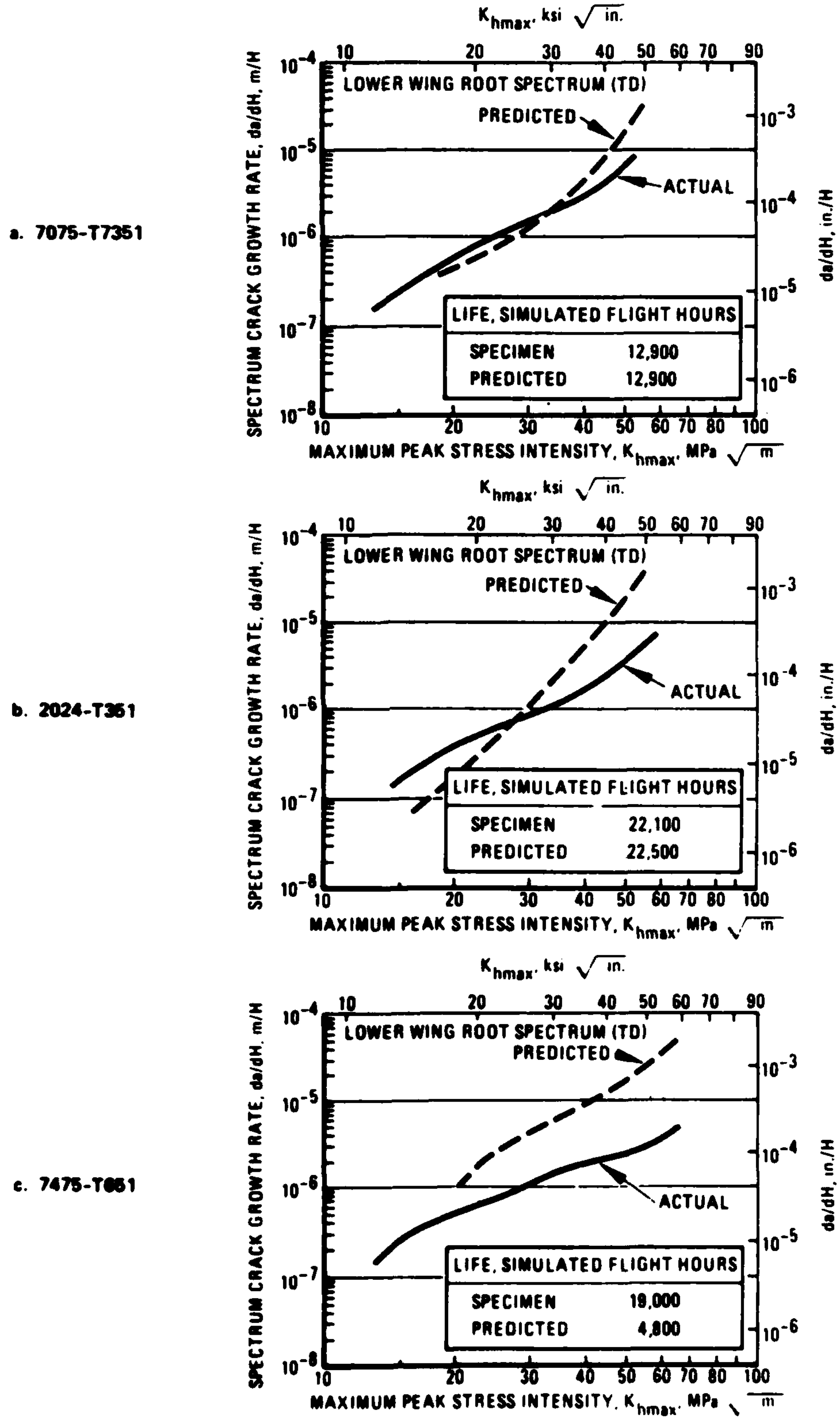

FIGURE D-1. PREDICTED AND ACTUAL SPECTRUM FCGR CURVES FOR TD SPECTRUM

APPENDIX E

EVALUATION OF SECOND HEAT OF 7475-T651

Alloy 7475-T651 had the best spectrum fatigue lives of all the 7000 series alloys which was not expected from the fracture toughness and constant-amplitude-fatigue behavior. To confirm this unexpected behavior Northrop and Alcoa at their own expense evaluated a second lot of 7475-T651.

In summary, this second lot did not have as good a spectrum fatigue behavior as the first lot, but still was the best of the six 7000 series alloys evaluated. The results are discussed in detail below.

The second lot was identified as 511348. The original first lot was identified as 511463.

E.1 TENSILE

The tensile properties at the T/2 location in the longitudinal direction were 598 MPa (86.7 ksi) ultimate strength, 550 MPa (79.8 ksi) yield strength, and 12 percent elongation and in the long transverse direction were 584 MPa (84.7 ksi) ultimate stength, 530 MPa (76.9 ksi) yield strength, and 14 percent elongation. In the longitudinal direction the strengths are about 11 MPa (2 ksi) higher than the first lot and the elongation is the same.

E.2 TOUGHNESS

Toughness was measured using a slow bend Charpy test at the T/2 location. The toughness in the L-T direction was 49.2 MPa m (44.8 ksi $\sqrt{\text{in.}}$) and in the T-L orientation was 41.4 MPa $\sqrt{\text{m}}$ (37.7 ksi $\sqrt{\text{in.}}$). These values cannot be directly compared to those obtained for the first lot using ASTM E399 procedures.

E.3 FATIGUE CRACK GROWTH RESULTS UNDER CONSTANT-AMPLITUDE LOADING

Data are shown in Figure E-1. At K less than about 7 MPa $\sqrt{m}$ the FCG rates for the second lot are faster.

E.4 SPECTRUM TEST RESULTS

A single test was performed for each of the five spectrums, TD, TDR, TC, TCR, and TCZ.

Graphs of crack length versus number of flight hours are shown in Figure E-2 and the graphs of spectrum FCG rates versus maximum peak stress intensity are shown in Figure E-3. A comparison of the spectrum fatigue crack growth lives is given in Table D-1. The lives for the first lot are longer than the second lot, except for the TCZ spectrum.

E.5 SUMMARY

The superiority of 7475-T651 over the other six materials was preserved, as a comparison of Table E-1 with Tables 7 and 9 will show.

TABLE E-1. SPECTRUM FATIGUE LIVES FOR THE TWO LOTS OF 7475-T651

σ_{hmax} = 145 MPa FROM a = 6mm TO FAILURE

SPECTRUM	LOT 1 (511463)	LOT 2 (511348)	DIFFERENCE*
TD	18,303 19,792	15,315	22
TDR	21,259	18,404	14
TC	14,744 15,141	14,188	5
TCR	19,387	15,991	19
TCZ	22,630 23,364	27,389	-17

$$* \text{ DIFFERENCE} = \frac{\text{LIFE (LOT 1) - LIFE (LOT 2)}}{\text{(LIFE (LOT 1) + LIFE (LOT 2))/2}} \times 100\%$$

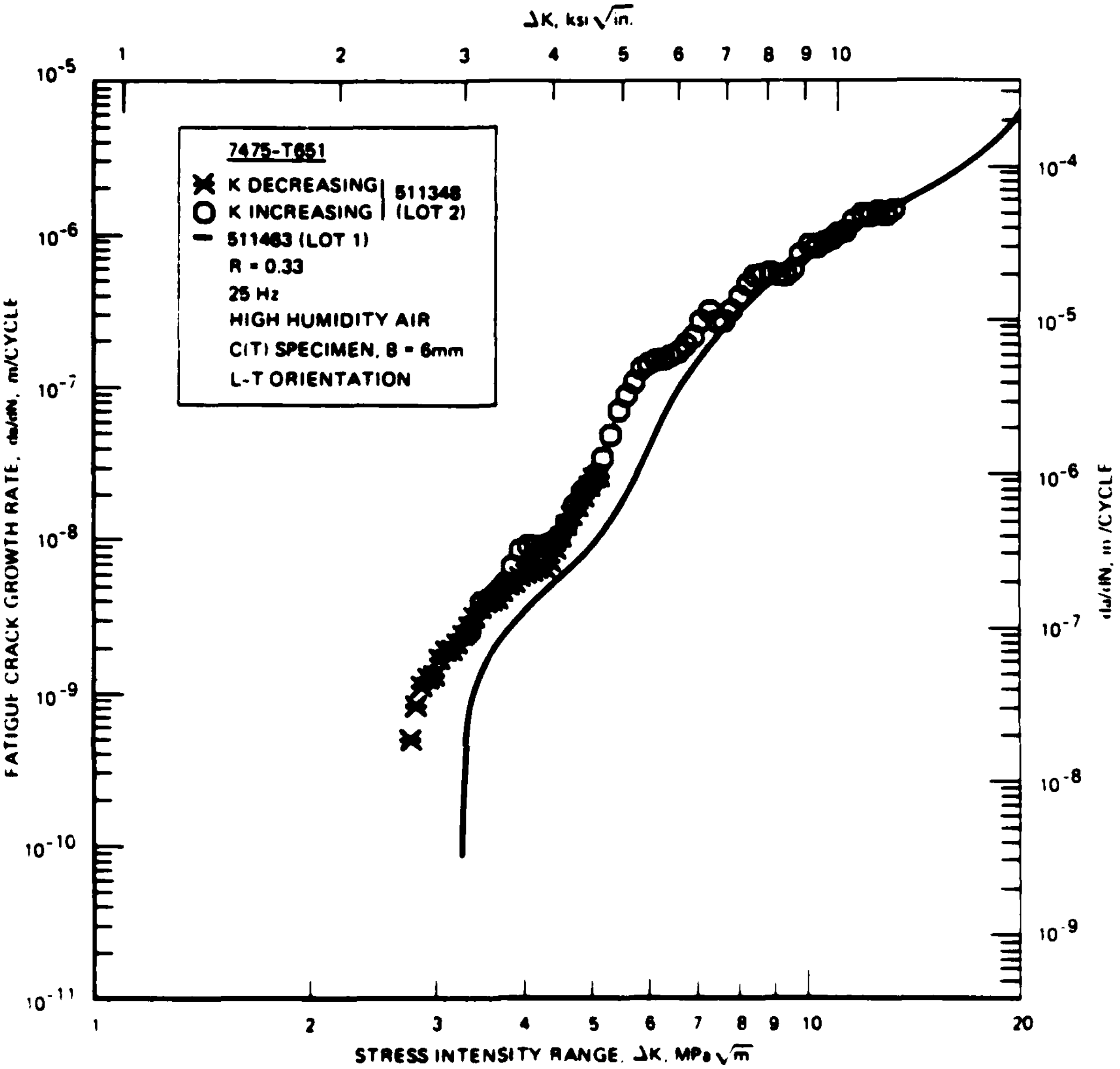

FIGURE E-1. CONSTANT-LOAD-AMPLITUDE FATIGUE CRACK GROWTH RATE DATA FOR 7475-T651

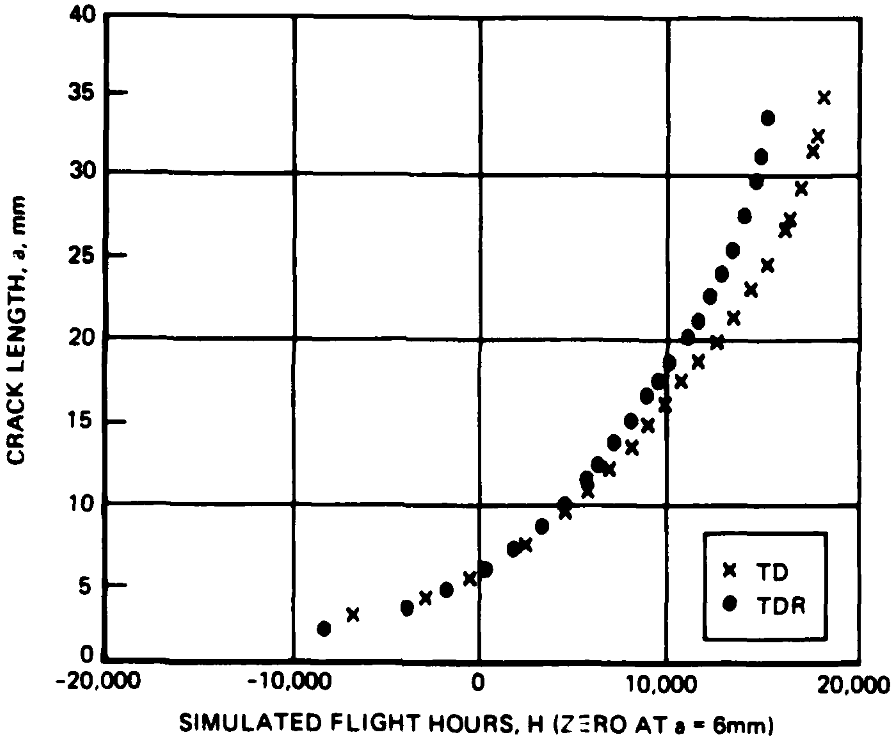

a. TD AND TDR SPECTRUMS

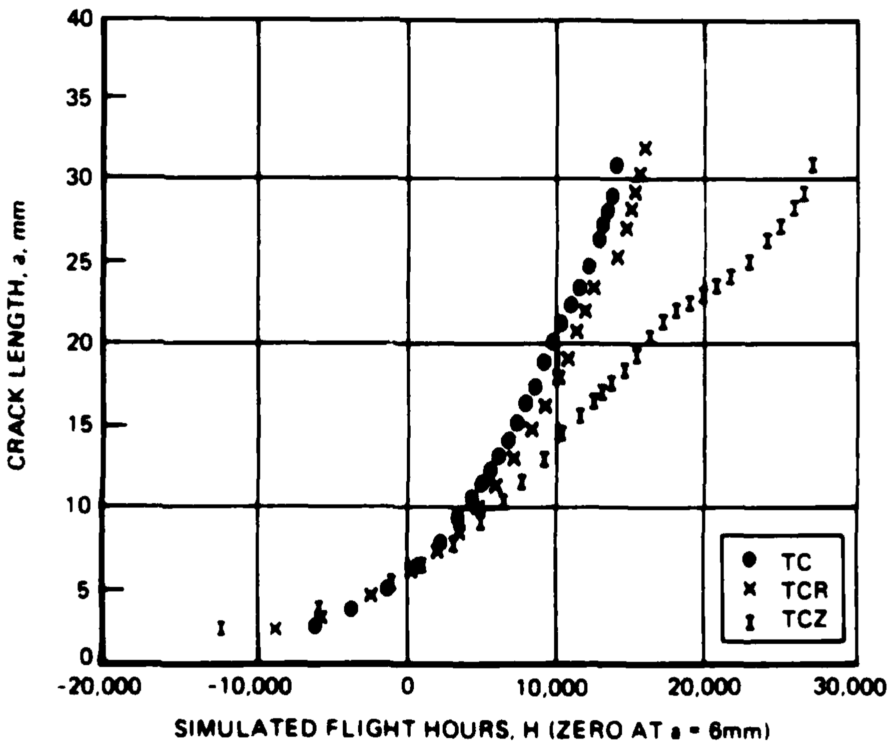

b. TC, TCR, AND TCZ SPECTRUM

FIGURE E-2. CRACK LENGTH VERSUS SIMULATED FLIGHT HOURS FOR 7475-T651, LOT 2

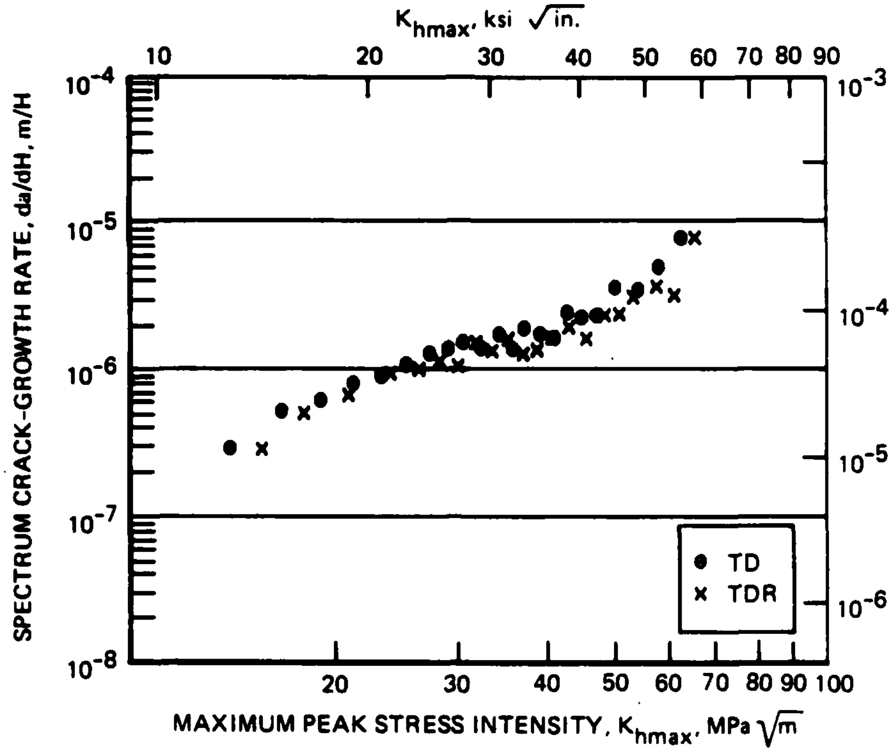

a. TD AND TDR SPECTRUMS

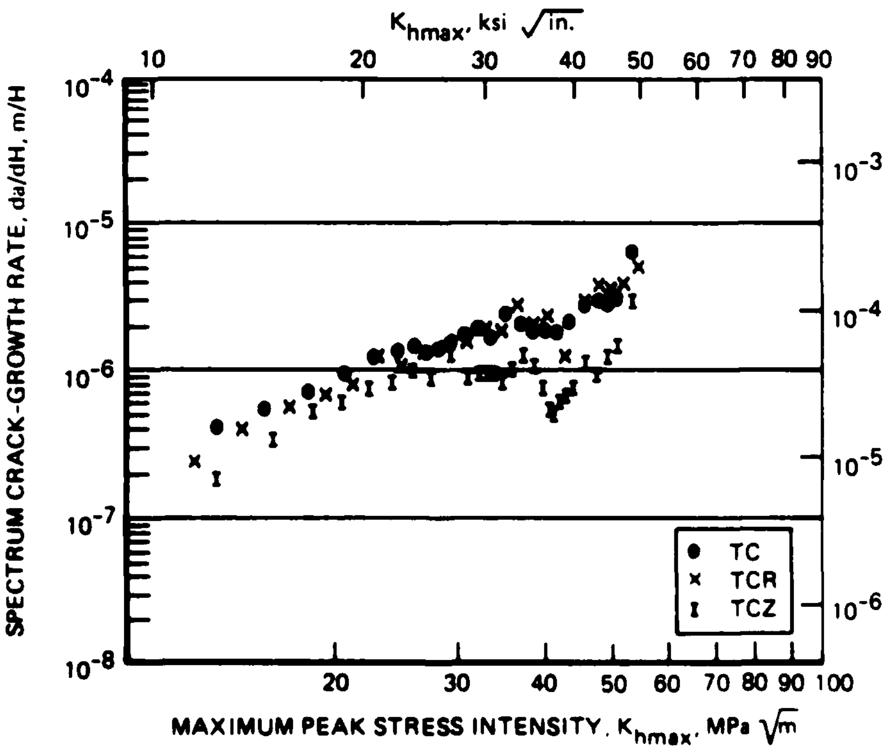

b. TC, TCR, AND TCZ SPECTRUMS

FIGURE E-3. SPECTRUM CRACK GROWTH RATE VERSUS MAXIMUM PEAK STRESS INTENSITY FOR 7475-T651, LOT 2

DISTRIBUTION LIST
(One copy only unless otherwise noted)

Commander
Naval Air Systems Command
Attn: Code AIR-5304B6 (2 copies)
Washington, D.C. 20361

AIR-7226 (4 copies)
AIR-5302 (1 copy)
AIR-310A (1 copy)
AIR-310B (1 copy)

Commander Naval Air Development Center
Attn: M. Thomas, Code 6063 (1 copy)
E. Tankins, Code 6063 (1 copy)
R. Mahorter, Code 6063 (1 copy)
Warminister, PA 18974

Commander
Naval Sea Systems Command
Code 05R
Department of the Navy
Washington, D.C. 20361

Commander
Naval Weapons Center
Code 5516
China Lake, CA 93555

Commander
Naval Surface Weapons Center
Metallurgy Div. -R32-D. Divecha
White Oak,
Silver Spring, MD 20910

Chief of Naval Research
Code ONR 423
ONR 431
800 N. Quincy Street
Arlington, VA 22217

Director
Naval Research Laboratory
Attn: Codes 6300 (1 copy)
6370 (1 copy)
6390 (1 copy)
Washington, D.C. 20375

Air Force Wright Aeronautical Laboratory
Attn: Code LLM (1 copy)
LLN (1 copy)
Metals Branch, Mfg. Tech Div (1 copy)
Wright-Patterson AFB
Dayton, OH 45433

Army Aviation Systems Command
P.O. Box 209
Attn: Mr. R. Vollmer-AMSAV-FRE
St. Louis, MO 63166

Army Research & Tech. Lab
Applied Technology Lab
DAVDL-ATL-ATS
Attn: T. Mazza
Ft. Eustis, VA 232604

Army Research Office
Box CM, Duke Station
Attn: Metallurgy & Ceramics Div
Durham, NC 27706

Army Mat'ls & Mech. Research Ctr
Attn: Dr. George Thomas
Watertown, MA 02171

Defense Advanced Research Project Agency
Attn: Dr. B.A. Wilcox Code 641
1400 Wilson Boulevard
Arlington, VA 22209

NASA
Ames Research Center
Code 240-10
Moffett Field, CA 94035

NASA Jet Propulsion Laboratory
4800 Oak Grove Drive
Pasadena, CA 91103

NASA
Langley Research Ctr
Attn: R.A. Pride
Langley Station, MS 15d
Hampton, VA 23365

Air Force Office of
Scientific Research
Dept. of the Air Force
Bolling Air Force Base
Washington, D.C. 20322

U.S. Department of Energy
Division of Reactor Research
& Technology
Attn: A. Van Echo
Mail Station B-107
Washington, D.C. 20545

National Academy of Sciences
National Materials Advisory Board
2101 Constitution Ave.
Attn: Dr. J.C. Lane
Washington, D.C. 20418

National Science Foundation
1800 G St., N.W.
Washington, D.C. 20550

Battelle Memorial Institute
Mfg. & Design Interaction
Attn: Dr. Bryan R. Noton
505 King Ave.
Columbus, OH 43201

Bell Helicopter Co.
Adv. Sys. Programs
Attn: James Kenna
P.O. Box 482
Ft. Worth, TX 76101

The Boeing Company
Aerospace Division
P.O. Box 3707, M/S 73-43
Attn: Mr. Rod Boyer
Seattle, WA 98124

Boeing Company
Vertol Division/MS P62-06
Attn: R. Pinckney
P.O. Box 95006
Philadelphia, PA 19142

EXXON Materials Division
Attn: Jerry Dixon
P.O. Box 95006
Raleigh, NC 27625

NASA
Marshall Space Flight Ctr
Attn: R. Schwinghamer
Huntsville, AL 35812

General Dynamics
Attn: C.F. Herndon
P.O. Box 748, MS 2830
Ft. Worth, TX 76101

General Dynamics Materials
Research
Attn: W.G. Scheck
P.O. Box 80847, MZ 640-00
San Diego, CA 92138

Grumman Aerospace Corp.
MS AD-12, Materials & Proc. Dept.
Attn: R.J. Herizman
South Oyster Bay Road
Bethpage, NY 11714

Grumman Aerospace Corp.
Ad. Mtls & Process Div.
Attn: Carl Micillo
Dept. 447, Plan 12
Bethpage, NY 11714

Hughes Aircraft Co.
Components & Materials Lab
Attn: L.B. Keller
Bldg. 6, Main Station, D-134
Culver City, CA 90230

Kaman Aerospace Corp.
Matl's & Process Engineering
Attn: A.S. Falcone
Old Windsor Road
Bloomfield, CT 06002

LTV Aerospace Corp.
Vought Systems Division
P.O. Box 5907
Attn: Mr. A.E. Hohman, Jr.
Dallas, TX 75222

Lockheed California Co.
Department 76-31 Bldg. 63
Attn: R. Kaseko/J. Pengra
Burbank, CA 91520

Lockheed Missile & Space Co., Inc.
Dept. 86-73
Attn. F.B. Yarborough
P.O. Box 504, Bldg. 153
Sunnyvale, CA 94088

Martin Marietta Corp.
Denver Division
Attn: Dr. A. Feldman
P.O. Box 179, MZ 1630
Denver, CO 80201

McDonnell Douglas Aircraft Co.
Mrg. R&D Dept (MS1-22)
Attn: Robert Zwart
3855 Lakekwood Blvd.
Long Beach, CA 90846

McDonnell Douglas Corporation
Engineering Division
Attn. B.B. Leonard
5301 BOLSA/MS A3-248/13-3
Huntington Beach, CA 92847

McDonnell Douglas Research Labs
P.O. Box 516
Attn: Dr. D.F. Ames
Dr. Charles Whitsett
St. Louis, MO 63166

Northrop Corporation
Attn: E. Jaffe
One Northrop Ave
Hawthorne, CA 90250-3277

Rockwell International Corp.
Attn. M. Mahoney
Science Center
1049 Camino Dos Rios
Thousand Oaks, CA 91830

Sikrosky Aircraft
Mfg. Engineering Dept.
Attn. J.D. Ray
North Main Street
Stratford, CT 06602

United Technologies Company
Research Center
400 Main Street
East Hartford, CT 06108

Kaiser Aluminum Chemical Corporation
Aluminum Division of Research
Center for Technology
P.O. Box 870
Pleasanton, CA 94566
Attn: T.R. Prichett

Reynolds Metals Company
Metallurgical Research Division
4th and Canal Streets
Richmond, CA 23219
Attn: Dr. Grant Spangler

Professor R. Ritchie
Department of Materials Science
and Mineral Engineering and
Lawrence Berkeley Laboratory
University of California
Berkeley, CA 94720

Professor S. Suresh
Brown University
Division of Engineering
Providence, RI 02912

Dr. E.A. Starke, Jr.
School of Engineering and Applied Science
University of Virginia
Charlottesville, VA 22903

Prof. A.J. McEvily
Department of Metallurgy
U-136
University of Connecticut
Storrs, CT 06268

Southwest Research Institute
8500 Culebra Road
P.O. Box 28510
San Antonio, TX 78284
Attn: Mr. J. Fitzgerald
Dr. D. Davidson

Aluminum Company of America
1200 Ring Bldg.
Washington, D.C. 20036
Attn: Mr. G. Barthold

Aluminum Company of America
Alcoa Center, PA 15069
Attn: Mr. Paul L. Mehr

D. Brook
123 Meadow Drive
Patafkala, OH 43062

Roy L. Hewitt, P.Engr., PhD.
Research Officer
Structures and Materials
Laboratory
National Aeronautical
Establishyment
Montreal Road
Ottawa, Canada
K1A OR6

Prof. J. Schijve
Delft University of Technology
Dept of Aerospace Engineering
P.O. Box 5058
2600 GD Delft
The Netherlands

Anders F. Blom, PhD.
The Aeronautical Research
Institute of Sweden
P.O. Box 11021
S-161 11 Bromma, Sweden

Douglas Aircraft Company
3855 Lakewood Blvd.
Long Beach, CA 90808
Attn: P.R. Abelkis
Mail Code 36-90
Dept. C1-E84

Douglas Aircraft Company
3855 Lakewood Blvd.
Long Beach, CA 90846
Attn: Dr. David Cho
Mail Code W5-20

Dr. Richard Hertzberg
Lehigh University
Bethlehem, PA 18015

Metals & Ceramics Info. Center
Battelle, Columbus Laboratories
505 King Avenue
Columbus, OH 43201

END

6-81

DTIC